# Imaging Diagnosis of TBI

2

Tuong H. Le, Shirley I. Stiver, and Alisa D. Gean

**Abstract**

Fundamentals and recent advances in imaging techniques and selection paradigms for the diagnosis of traumatic brain injury (TBI) will be discussed. Characteristic imaging findings for common TBI lesions will be described. Computed tomography (CT) is the modality of choice for the initial assessment of acute TBI. Magnetic resonance imaging (MRI) is recommended for patients with acute TBI when the neurological findings are unexplained by CT. MRI is the modality of choice for the evaluation of subacute and chronic TBI. Advanced MR techniques, such as diffusion weighted imaging, can improve the identification of otherwise occult lesions, especially with mild TBI.

**Keywords**

Imaging • Traumatic brain injury • Blast-induced injury • CT • MRI

T.H. Le, M.D., Ph.D.
Department of Radiology, San Francisco General Hospital, University of California, San Francisco, San Francisco, CA 94110, USA

S.I. Stiver, M.D., Ph.D.
Department of Neurological Surgery, San Francisco General Hospital, University of California, San Francisco, San Francisco, CA 94110, USA

Brain and Spinal Injury Center (BASIC), San Francisco General Hospital, San Francisco, CA 94110, USA

A.D. Gean, M.D. (✉)
Department of Radiology, San Francisco General Hospital, University of California, San Francisco, San Francisco, CA 94110, USA

Department of Neurological Surgery, San Francisco General Hospital, University of California, San Francisco, San Francisco, CA 94110, USA

Brain and Spinal Injury Center (BASIC), San Francisco General Hospital, San Francisco, CA 94110, USA

Division of Neuroradiology, 1X55, San Francisco General Hospital, 1001 Potrero Avenue, San Francisco, CA 94110, USA
e-mail: alisa.gean@radiology.ucsf.edu

J.W. Tsao (ed.), *Traumatic Brain Injury: A Clinician's Guide to Diagnosis, Management, and Rehabilitation*,
DOI 10.1007/978-0-387-87887-4_2, 

## Introduction

*Traumatic brain injury* (TBI) refers to injury to the intracranial structures following physical trauma to the head. TBI can be classified into *primary* and *secondary* injuries. Primary injuries are the result of direct trauma to the head and occur at the moment of impact. Secondary injuries arise as sequelae due to activation of excitatoxic, oxidative, inflammatory and other signaling cascades following the primary injury. Secondary injuries are potentially preventable and treatable, whereas primary injuries, by definition, have already occurred by the time the patient first presents for medical attention. TBI can be further divided according to *location* (intra-axial or extra-axial) and also by the nature of the *mechanism* of injury (penetrating/open or blunt/closed). The severity of TBI is classified clinically according to the universally accepted Glasgow Coma Scale (GCS). Patients presenting with GCS<=8 are designated as having a severe TBI, those with GCS between 9 and 12 are categorized as moderate injuries, and mild TBI (mTBI) encompasses patients with a GCS 13–15 (Teasdale and Jennett 1974). From the moment of impact, TBI is a dynamic process with varying therapeutic windows, and early diagnosis and intervention are imperative for favorable outcomes.

Diagnosis and management of TBI requires a multi-disciplinary approach, starting with a detailed history and physical examination, followed by appropriate diagnostic imaging, and subsequent medical and/or surgical intervention as deemed necessary. The goals of imaging include identification of treatable injuries, recognition of sources of potential secondary damage, and analyses of factors that may provide useful prognostic information for long-term outcome. Advances in medical imaging technology have resulted in an explosion of novel imaging modalities that have improved the sensitivity and specificity for early detection of TBI and added a host of valuable prognostic indicators and signs to help guide patient management. Consequently, clinicians are faced with the difficult task of selecting the most appropriate diagnostic test from an array of available imaging techniques. These decisions are of vital importance for optimal management, especially for injuries that require aggressive and timely intervention. In this chapter, recent advances in imaging techniques and selection paradigms for the diagnosis of TBI will be discussed. Characteristic imaging findings for individual lesions observed in TBI will be described in detail, including a discussion of the unique imaging features of blast-induced brain injury.

## Imaging Selections

### Conventional Radiography

Skull fracture, with or without signs of neurological injury, is an independent risk factor for a neurosurgically relevant intracranial lesion (Munoz-Sanchez et al. 2009). Therefore, in the setting of clinically occult TBI, the diagnosis of skull fracture serves to alert the clinician to the possibility of an immediate or delayed neurologically relevant intracranial lesion. Conventional radiography itself (film or digital) is not sensitive for detection of intracranial pathology and should not be performed to evaluate parenchymal damage in TBI (Bell and Loop 1971; Hackney 1991; Masters 1980). In mTBI, skull films rarely demonstrate significant findings; and in severe TBI, the lack of abnormality on skull films does not exclude major intracranial injury (Adams 1991). Patients who are at risk for acute intracranial injury, even without clinical evidence of a skull fracture, should be imaged by computed tomography (CT).

### Computed Tomography

In the setting of acute head trauma, a non-contrast CT is recommended for patients with moderate and severe TBI (GCS ≤ 12) and in any patient with evidence of a penetrating injury. CT is not indicated for mTBI (GCS > 12) unless the patient meets one of the following criteria, that also

**Table 2.1** New Orleans Criteria for mTBI—A non-contrast CT of the head is indicated if the patient meets one or more of the following criteria

| |
|---|
| Headache |
| Vomiting |
| Age > 60 years |
| Drug or alcohol intoxication |
| Persistent ante-grade amnesia (short term memory deficits) |
| Visible trauma above the clavicle |
| Seizure |

**Table 2.2** Canadian CT Head Rule for mTBI—A non-contrast CT of the head is indicated if the patient meets one or more of the following criteria

| |
|---|
| GCS < 15 two hours after injury |
| Suspected open or depressed skull fracture |
| Any sign of basal skull fracture |
| Two or more episodes of vomiting |
| Age ≥ 65 years |
| Amnesia before impact of 30 min or more |
| Dangerous mechanism (i.e., pedestrian struck by motor vehicle, occupant ejected from motor vehicle, or a fall from a height of at least 3 ft or five stairs) |

include those recommended by the New Orleans Criteria (Table 2.1) and the Canadian CT Head Rule (Table 2.2), which consist of age > 60 years, persistent neurologic deficit(s), headache or vomiting, amnesia, loss of conciousness ≥ 5 min, depressed skull fracture, bleeding diathesis or anticoagulation therapy (Haydel et al. 2000; Jagoda et al. 2002; Stiell et al. 2001a, b, c). CT is the primary modality of choice because it is fast, widely accessible, and there are few contraindications to a non-contrast CT scan. Pregnancy, especially in the first trimester, is a relative contraindication for a CT scan. In the setting of TBI, one needs to balance the risks of the CT against how the information from the scan might alter the patient's management. Unlike Magnetic resonance imaging (MRI), CT can easily accommodate life-support and monitoring equipment. In addition, CT is superior to MRI for the dectection of skull fractures and radio-opaque foreign bodies. In fact, MRI is contraindicated in the presence of certain foreign bodies. Non-contrast CT scans provide rapid and accurate detection of space-occupying hematomas and associated mass effect, together with signs that reliably flag impending complications of herniation that would require immediate medical and/or surgical intervention. Intravenous contrast administration should not be performed without a baseline non-contrast exam because the contrast can both mask and mimic underlying hemorrhage. Addition of contrast, after the non-contrast scan, can, however, detect active extravasation and alert the clinician to a highly unstable lesion that has the risk for rapid enlargement.

*CT angiography* (CTA) utilizes iodinated intravenous contrast to delineate the vascular structures at high (sub-millimeter) resolution. CTA is best performed with multi-detector CT (MDCT) and rapid bolus contrast injection using vessel tracking technique. Typical imaging parameters include a slice thickness of 1.25 mm, with a 0.625 mm overlap, and a bolus injection rate between 3 and 4 mL/s. In suspected vascular injury, such as in the setting of a fracture traversing the carotid canal or venous sinus, CTA can serve as a useful screening method for vascular injuries such as carotid dissections, fistulas, and venous stenoses or occlusions (Enterline and Kapoor 2006).

*Dynamic perfusion CT* measures brain hemodynamics by tracking transient attenuation changes in the blood vessels and brain parenchyma during the first-pass of an intravenously-injected contrast bolus. Perfusion CT involves continuous cine scanning with a scan interval of 1 s and a total scanning duration of 40–45 s (Wintermark et al. 2005). Maps of cerebral blood volume (CBV), mean transit time (MTT), and cerebral blood flow (CBF) are generated from a voxel-by-voxel analysis of the change in attenuation over time. In severe trauma, CT perfusion has been shown to provide independent prognostic information regarding functional outcome with normal brain perfusion or hyperemia correlating with favorable outcome, and oligemia associated with unfavorable outcome (Wintermark et al. 2004). One potential limitation of dynamic perfusion CT is limited anatomic coverage, because only a few slices of the brain can be imaged on some CT scanners during the 1-s time acquisition

window. Wider coverage can be achieved using a 40-mm-wide detector and toggling table technique or by the more recent availability of scanners with more multislice detectors (Siebert et al. 2009; Youn et al. 2008). Another limitation of CT perfusion is the additional radiation exposure that accompanies cine imaging.

## Magnetic Resonance Imaging

### Conventional MRI

MRI may be indicated in patients with acute TBI if the neurologic findings are unexplained by the CT imaging. Routine MR imaging typically includes T1- and T2-weighted spin-echo, gradient-echo, and inversion recovery MR sequences. MRI is preferred over CT for subacute and chronic TBI because of its superior sensitivity to older blood products. MR also demonstrates increased dectection of grey and white matter injury as well as lesions, especially shear injury, in the brainstem. MRI is comparable to CT in the detection of acute epidural and subdural hematomas (Gentry et al. 1988; Orrison et al. 1994). Compared to CT, MRI is more sensitive for detection of subtle extra-axial "smear" (i.e., very thin layer) collections, non-hemorrhagic lesions, and brainstem injuries. Fluid attenuated inversion recovery (FLAIR) MRI can also be more sensitive to subarachnoid hemorrhage (Noguchi et al. 1997; Woodcock et al. 2001).

*Fluid Attenuated Inversion Recovery* (FLAIR) imaging suppresses the bright cerebrospinal fluid (CSF) signal typically seen on conventional T2-weighted images, thereby improving the conspicuity of focal cortical injuries, white matter shearing injuries, and subarachnoid hemorrhages. Sagittal and coronal FLAIR images are particularly helpful in the detection of diffuse axonal injury (DAI) involving the corpus callosum and the fornix, two areas that can be difficult to evaluate on routine T2-weighted images (Ashikaga et al. 1997). Abnormal high signal in the sulci and cisterns of ventilated patients receiving a high inspired oxygen fraction greater than 0.60 ($\text{inspired oxygen fraction} = [\text{flow rate}_{\text{air}} \times 0.21 + \text{flow rate}_{\text{oxygen}}]/[\text{flow rate}_{\text{air}} + \text{flow rate}_{\text{oxygen}} + \text{flow rate}_{\text{nitrous oxide}}]$) can be observed on FLAIR sequences in normal, uninjured patients and should not be mistaken for subarachnoid hemorrhage (Frigon et al. 2002).

*Gradient-Recalled-Echo (GRE) T2*-weighted* imaging is highly sensitive to the susceptibility changes among tissues. The presence of blood breakdown products from brain injury, such as methemoglobin, ferritin and hemosiderin, alters the local magnetic susceptibility of tissue, resulting in areas of signal loss on GRE T2*-weighted images. Because hemosiderin can persist indefinitely, its detection on GRE T2*-weighted images is especially useful for the evaluation of remote TBI. Small foci of hemosiderin can, however, sometimes be resorbed; therefore, the lack of hemosiderin on GRE T2*-weighted images does not rigorously exclude old hemorrhage (Messori et al. 2003).

### Advanced MRI Methods

*Susceptibility-Weighted Imaging* (SWI) further amplifies the susceptibility changes among tissues and blood products by combining magnitude and phase information from a high-resolution, velocity-compensated 3D T2*-weighted gradient echo sequence (Haacke et al. 2004). Conventional GRE T2*-weighted MRI relies only on the magnitude images and ignores the phase images, the latter of which contain valuable information regarding tissue susceptibility differences. In SWI, phase images are unwrapped and high-pass filtered to highlight phase changes. These are then converted to "*mask*" images that are multiplied with information from the corresponding magnitude images. The increase in tissue magnetic susceptibility contrast afforded by SWI is significantly more sensitive to small hemorrhages. SWI is 3–6 times more sensitive than GRE T2*-weighted imaging for detection of hemorrhagic DAI (Babikian et al. 2005; Tong et al. 2003, 2004).

*Diffusion-Weighted Imaging* (DWI) measures the random microscopic motion of water molecules in brain tissue. DWI is very sensitive to alterations in the pattern of water molecule

movement that occurs following acute shear injury, and, thus, DWI has been particularly useful for the detection of DAI (Arfanakis et al. 2002; Huisman et al. 2003; Le et al. 2005; Liu et al. 1999; Niogi et al. 2008). DWI identifies more acute DAI lesions than fast spin-echo T2-weighted and/or GRE T2*-weighted images. Acute DAI lesions typically also show a reduced apparent diffusion coefficient (ADC), which measures the magnitude of water diffusion averaged over a 3-dimensional (3D) space. By comparison, chronic DAI lesions frequently demonstrate reduced fractional anisotropy (FA), which measures the preferential motion of water molecules along the white matter axons. The integrity of the white matter tracts can be further assessed with diffusion tensor imaging (DTI) with 3D tractography (Conturo et al. 1999; Mori and van Zijl 2002). Images of the white matter fiber tracts are generated based on the direction of fastest diffusion of water molecules, which is assumed to correspond to the longitudinal axis of the fiber tract. Unfortunately, there is still considerable variability in techniques used to prepare images of the fiber tracts using DTI tractography. Abnormalities identified within the white matter tracts created with DTI need to be carefully assessed for the parameters, technical expertise, and reproducibility of the image processing to distinguish true lesions from artifacts.

*MR Spectroscopy* (MRS) allows for in vivo measurement of the relative amount of metabolites in brain tissue. Common brain metabolites that are measured with proton ($^1$H) MRS include *N*-acetylaspartate (NAA), creatine (Cr), choline (Cho), glutamate, lactate, and myoinositol. NAA is a cellular amino acid and is a marker of neuronal health. Creatine is a marker of energy metabolism and cellular density. Creatine is especially abundant in glial cells, and can serve as a marker for post-traumatic gliosis. Cho is a marker for membrane disruption, synthesis or repair. An increase in Cho is observed in myelin injury. MRS can detect abnormalities that may not be visible on conventional MRI (Garnett et al. 2000a, b). A reduction of NAA and an elevation of Cho have been shown to correlate with the severity of TBI, as measured by the GCS and duration of post-traumatic amnesia (Garnett et al. 2000a). A reduction in the NAA:Cr ratio also correlates with a worse prognosis following TBI (Sinson et al. 2001).

*Magnetization Transfer Imaging* (MTI) exploits the longitudinal (T1) relaxation coupling between bound (hydration) protons and free water (bulk) protons. Protons that bind to macromolecules are selectively saturated using an off-resonance saturation (radiofrequency) pulse. These bound protons subsequently exchange longitudinal magnetization with free water protons. The magnetization transfer ratio (MTR), a relative measure of the reduction in signal intensity due to the magnetization transfer (MT) effect, provides a quantitative measure of the structural integrity of tissue. In TBI, a reduction of the MTR correlates with a worse clinical outcome (Sinson et al. 2001).

*Perfusion MRI* employs either dynamic susceptibility contrast (DSC) or arterial spin labeling (ASL) imaging. In DSC-MRI, following intravenous injection of gadolinium contrast, continuous cine imaging of fast (echo-planar) T2*-weighted images is performed. As the contrast passes through the tissues, it causes susceptibility changes and associated reduction of signal intensity on T2*-weighted images. Maps of CBF, CBV, and MTT can be generated using pixel-by-pixel analysis of the signal changes. ASL-MRI is an alternative, safe, convenient noninvasive method to measure CBF by using the water molecules in arterial blood as a natural diffusible tracer. With ASL-MRI water molecules in inflowing arteries are "*labeled*" using radiofrequency (inversion or saturation) pulses proximal to the tissue of interest. Images of the tissue of interest are acquired after a short delay (usually 1 s) that allows the labeled blood water to flow into the imaging slices. The perfusion parameters are calculated by pair-wise comparison with baseline control images acquired without spin labeling. Based on the tracer half-life of blood T1, absolute CBF can be quantified. ASL scans

can be repeated as often as necessary during the same scanning session without any added risks or cumulative effects.

### Magnetic Source Imaging

Magnetic source imaging (MSI) utilizes magnetoencephalography (MEG) to localize weak magnetic signal generated by neuronal electrical activity. Electrical currents flowing within dendrites give rise to a surrounding magnetic field that can be measured by superconducting quantum interfering devices (SQUID). MEG provides a selective reflection of activity in dendrites oriented parallel to the skull surface. MSI integrates anatomic data obtained with conventional MRI and electrophysiological data obtained with MEG. So far, only two MSI studies have been published (Lewine et al. 1999, 2007). These MSI studies showed excessive abnormal low-frequency magnetic activity in mTBI patients with post-concussive syndrome. Additional research is warranted before MSI can be adopted in the clinical setting.

### Positron Emission Tomography

Positron emission tomography (PET) utilizes positron-emitting isotopes, commonly 15-oxygen ($^{15}$O) to measure cerebral perfusion and oxygen metabolism, and 2-fluoro-2-deoxy-D-glucose ($^{18}$F-FDG) to measure cerebral glucose metabolism. $^{15}$O-PET can define potential ischemic areas after brain injury, which is associated with poor outcome (Coles et al. 2004a, b; Menon 2006). $^{18}$F-FDG can evaluate glucose metabolism in vivo. Acutely injured brain cells show increased glucose metabolism following severe TBI due to intracellular ionic perturbation (Bergsneider et al. 2001). Following the initial hyperglycolysis state, injured brain cells show a prolonged period of regional hypometabolism. Since glucose metabolism reflects neuronal activity, regional hypometabolism implies neuronal dysfunction. For that reason, $^{18}$F-FDG has the potential to reveal cerebral dysfunction in regions that would appear otherwise "normal" on CT or MRI (Kato et al. 2007; Nakashima et al. 2007). Although $^{18}$F-FDG PET imaging has made great progress in the field of oncology, it is relatively expensive and is not widely available for the evaluation of TBI.

### Single Photon Emission Tomography

Single photon emission tomography (SPECT) uses gamma-emitting isotopes, e.g., $^{133}$Xe and technetium-99-m-hexamethyl-propylamine-oxime ($^{99}$Tc-HMPAO), to measure CBF. It can potentially provide a better long-term prognostic predictor in comparison to CT or conventional MRI (Newton et al. 1992). For example, a worse prognosis has been associated with multiple CBF abnormalities, larger CBF defects, and CBF defects within the brainstem, basal ganglia, temporal and parietal lobes. SPECT can also show areas of perfusion abnormality following head trauma that are "normal" on conventional CT and MRI (Kinuya et al. 2004). However, due to its low spatial resolution, SPECT is less sensitive in detecting small lesions that are visible on MRI.

## Imaging Findings

### Missile and Penetrating Injury

In the United States, the majority of penetrating injuries are due to assaults and suicide attempts (Gean et al. 1995). More than 80% of gunshot wounds to the head penetrate the scalp and skull, and 80% of these patients die (Awasthi 1992). Missile injuries result in various forms of brain damage, depending on the mass, velocity and shape of the missile (Lindenberg and Freytag 1960). Missile injury is classified as superficial, depressed, penetrating, or perforating. In *superficial missile injury*, the weapon remains extracranial and the skull is intact, but brain damage can still occur as a result of the initial impact force (Fig. 2.1). High velocity, small shotgun fragments can cause intracranial injury even if they are superficial because the applied energy depends not only on the mass ($m$) but also on the

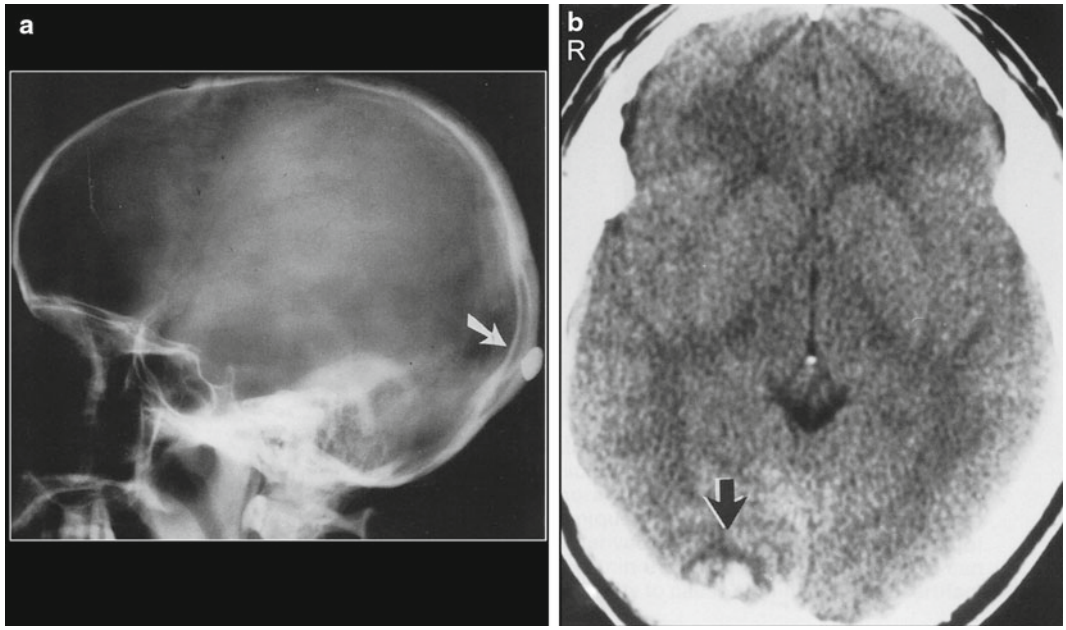


**Fig. 2.1** Superficial missile injury. (**a**) Lateral skull film shows a bullet lodged within the soft tissue overlying the occiput. (**b**) Non-contrast axial CT, performed after removal of the bullet, demonstrates a subjacent left occipital lobe contusion (*arrow*). No fracture is identified on the "bone window" images (not shown). (Reprinted with permission from Gean AD. Imaging of head trauma. Philadelphia, PA: Williams & Wilkins-Lippincott; 1994, p. 191)

square of the velocity ($v$) (i.e., kinetic energy $= \frac{1}{2}mv^2$). With increases in velocity, an extracranial missile may have enough impact to cause a depressed skull fracture and subjacent parenchymal injury, resulting in a *depressed missile injury* (Fig. 2.2). However, the majority of ballistics penetrate skull, meninges, and brain, causing a *penetrating missile injury* (Awasthi 1992). The brain laceration caused by the missile is characteristically canalicular, with decreasing diameter from the entry site to the exit site. A high-velocity missile can generate enough shock wave damage to cause a contusion at a distance from the missile trajectory or even result in diffuse cerebral edema (Fig. 2.3). With even greater velocity, a missile can exit the contralateral side of the skull, resulting in a *perforating missile injury*. The exit site is usually larger than the entry site (Purvis 1966). Another distinguishing feature is that the inner table of the skull is beveled at the entry site while the outer table of the skull is beveled at the exit site (Fig. 2.4).

## Blunt Injury

### Primary Extra-Axial Injury

#### Pneumocephalus

*Pneumocephalus* (intracranial air) indicates a communication between the intracranial and extracranial compartments. Pneumocephalus can occur in the epidural (Fig. 2.6), subdural, intraventricular space or the brain parenchyma (pneumatocele). The most frequent cause of traumatic pneumocephalus is from a fracture of the posterior wall of the frontal sinus. With a calvarial-dural defect, rapid increases in pressure within the paranasal sinuses (e.g., from sneezing or coughing) may force air into the intracranial cavity. With a CSF leak, the decrease in intracanial pressure (ICP) also leads to a compensatory influx of air, resulting in pneumocephalus. Most cases of pneumocephalus resolve spontaneously. In rare instances, expanding tension pneumocephalus can cause mass effect, headache, stiff neck, stupor, and papilledema (Briggs 1974).

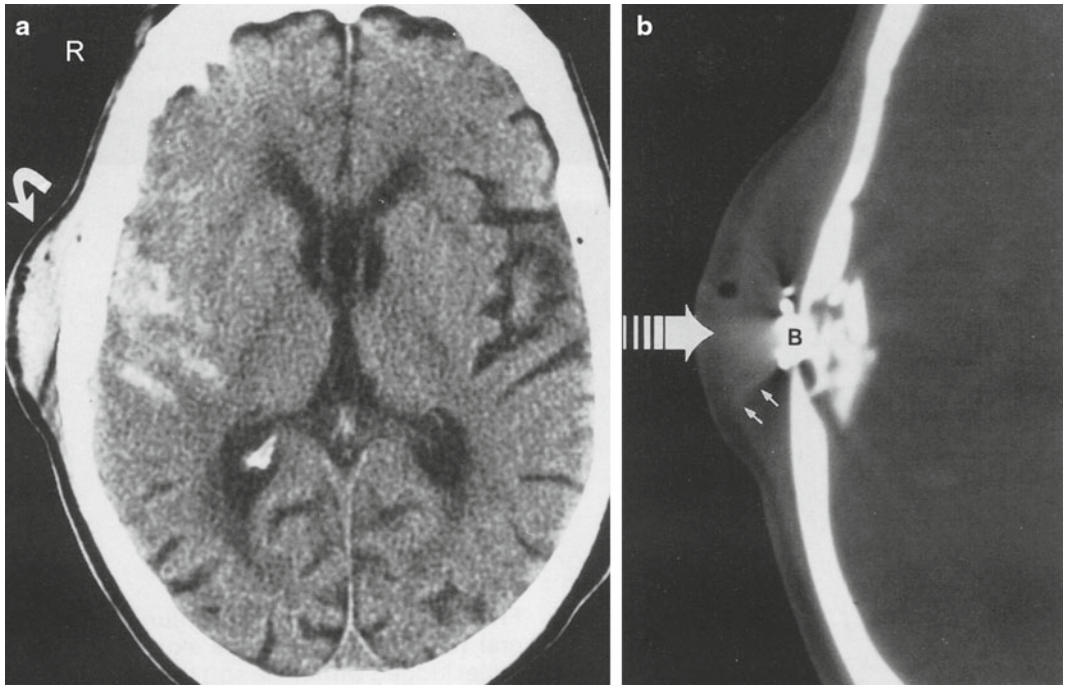


**Fig. 2.2** Depressed missile injury. (**a**) Non-contrast axial CT image demonstrates posterior right temporal scalp soft tissue swelling (*curved arrow*) and a subjacent temporal contusion, subarachnoid hemorrhage, and effacement of the frontotemporal sulci. (**b**) CT image displayed in bone window reveals a bullet fragment (B) lodged within the outer table of the skull. Multiple bone fragments from the inner table of the skull are noted. (Reprinted with permission from Gean AD. Imaging of head trauma. Philadelphia, PA: Williams & Wilkins-Lippincott; 1994, p. 192)

Tension pneumocephalus requires immediate intervention. On imaging, the air usually collects ventrally since most patients are scanned in the supine position.

### Epidural Hematoma

A hematoma that develops within the potential space located between the dura and the inner table of the skull is called an *epidural hematoma* (EDH). The EDH splits the dura from the inner table of the skull, forming an oval collection that can cause focal compression of the underlying brain. Because the EDH is subperiosteal, it rarely crosses cranial sutures, where the outer periosteal layer of the dura is firmly attached at sutural margins (Fig. 2.5) (Gean et al. 1995). At the vertex, however, where the periosteum is not tightly attached to the sagittal suture, the EDH can cross the midline.

EDHs are usually arterial in origin. Most EDHs occur at the coup site (i.e., the site of impact) and are usually associated with a skull fracture, commonly involving the temporal squamosa region where the fracture disrupts the partially embedded middle meningeal artery (Zee and Go 1998; Zimmerman et al. 1978). In children, EDHs may occur from stretching or tearing of meningeal arteries without an associated fracture. EDHs are less common in young children because the overall incidence of head trauma is lower the pediatric skull is more compliant, and the meningeal groove is more shallow. EDHs are also less common in the elderly because the dura in the elderly is more adherent to the inner table of the skull and is, therefore, not easily displaced.

On CT, an acute EDH appears as a well-defined biconvex hyperdense collection, with attenuation between 50 to 70 Hounsfield units (HU) (Fig. 2.6). On MRI, a thin dark line is observed at the inner margin of the EDH (Fig. 2.7). This line represents the two layers of displaced dura and confirms

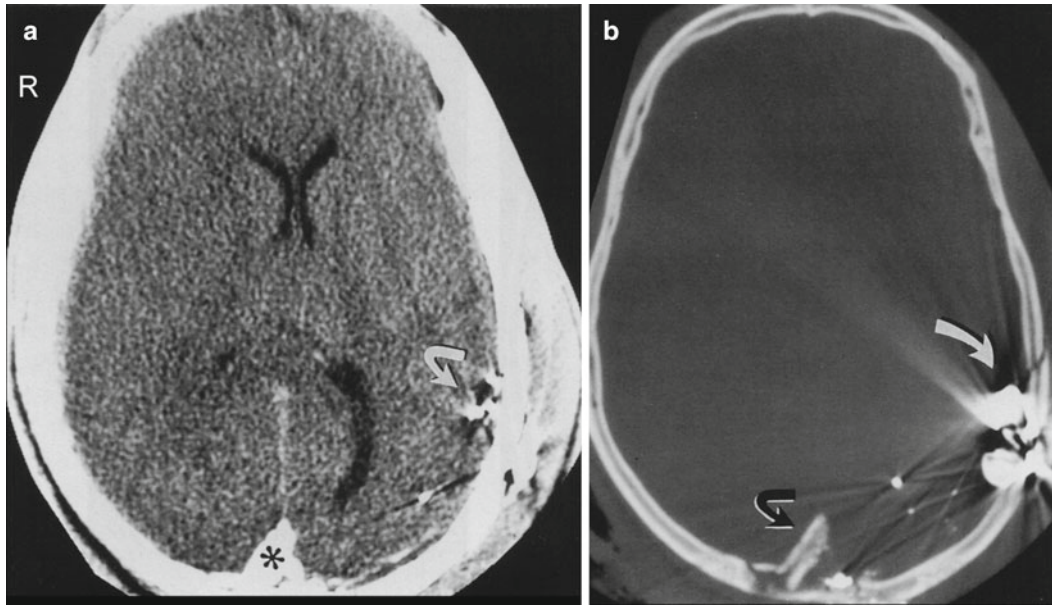


**Fig. 2.3** Penetrating missile injury. (**a**) Non-contrast axial CT image reveals several metallic fragments within the left parietal lobe (*arrow*) with associated overlying scalp soft-tissue swelling. There is effacement of the right occipital horn and complete loss of gray-white matter differentiation due to cerebral edema. A bone fragment projects into the superior sagittal sinus (*asterisk*). (**b**) The corresponding bone-window image demonstrates a displaced fracture fragment projecting into the superior sagittal sinus (*black arrow*). Note how the donor site for the fracture fragment is the inner table of the skull—a finding consistent with the clinical history that the patient was shot in the occiput. Multiple metallic fragments and a comminuted skull fracture are seen in the left parietal region (*white arrow*). The patient died several hours later. (Reprinted with permission from Gean AD. Imaging of head trauma. Philadelphia, PA: Williams & Wilkins-Lippincott; 1994, p. 193)

the epidural location of the hematoma. Inward displacement of the venous sinuses also serves as a clue that the hematoma is located within the epidural space. As is the case with hematomas elsewhere, the MR signal characteristics of the EDH correlate with the age of the blood products (Gomori et al. 1985; Fobben et al. 1989).

An important imaging finding of the EDH that correlates with a worse prognosis is the presence of low-density areas within the hyperdense hematoma (the "swirl sign"), thought to represent active bleeding (Fig. 2.8) (Al-Nakshabandi 2001; Greenberg et al. 1985). It forewarns expansion of an arterial EDH. Patients with an expanding EDH tend to present early, with a poorer GCS, and a higher mortality rate (Pruthi et al. 2009). Contrast extravasation within the low density areas of the EDH due to active hemorrhage from an underlying dural vessel laceration has also been reported (Kumbhani et al. 2009). Thus, active extravasation on CT may be another potential biomarker for EDH expansion, and may warrant more aggressive clinical management. Midline shift > 1 cm and brainstem distortion are additional imaging findings that often require aggressive management.

Venous EDHs are less common than arterial EDHs, and they occur due to bleeding from meningeal and diploic veins or from the dural sinuses. They tend to occur in three classic locations: (1) the posterior fossa from rupture of the torcula Herophili or transverse sinus (Fig. 2.9), (2) middle cranial fossa from disruption of the sphenoparietal sinus (Fig. 2.9), (Le and Gean 2009) and (3) vertex due to injury to the superior sagittal sinus or cortical veins (Gean et al. 1995). Unlike the arterial EDH, the venous EDH rarely expands beyond its initial size because of the lower pressure imposed by venous extravasation. The venous EDH is less frequently associated with a skull fracture than is the arterial EDH.

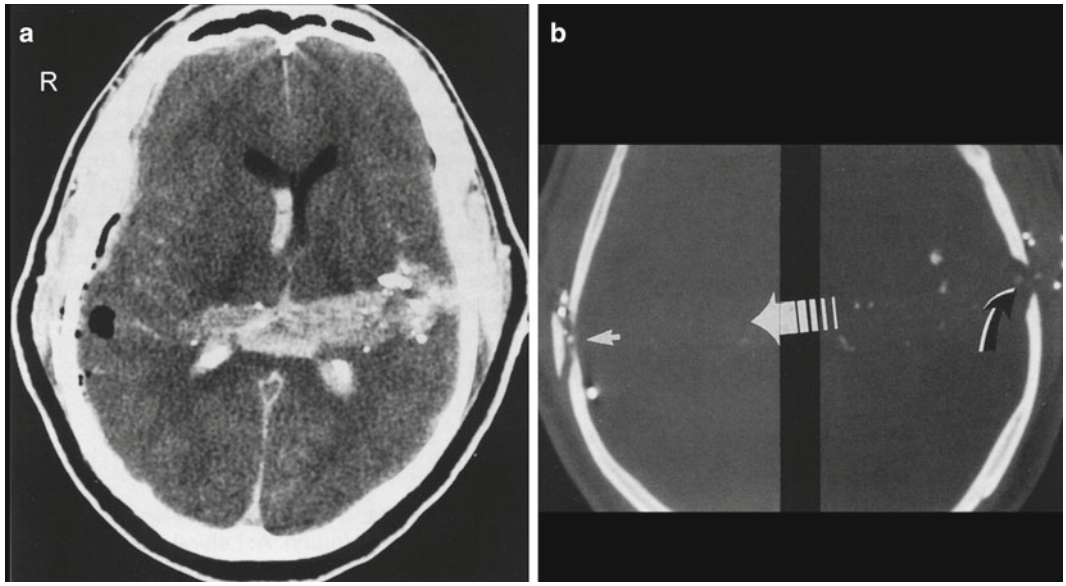


**Fig. 2.4** Perforating missile injury. (**a**) Non-contrast axial CT image demonstrates a left temporal gunshot wound that crosses the midline and ultimately exits the right temporal skull on a higher section. Note how the brain injury typically has a canalicular shape with a diameter that decreases from the site of entry to its exit. There is intraventricular hemorrhage, a small right subdural hematoma, and a small amount of pneumocephalus. (**b**) Corresponding bone-window images are spliced together to illustrate how the entry and exit sites can be distinguished by the location of the calvarial beveling. At the entry site (*black arrow*), the inner table of the skull is beveled. At the exit site, the outer table of the skull is beveled (*small white arrow*). In this example, only a few bullet fragments actually perforate the skull at the exit site. A wedge-shaped bone fragment from the outer table appears to have been lifted off the calvarial surface. (Reprinted with permission from Gean AD. Imaging of head trauma. Philadelphia, PA: Williams & Wilkins-Lippincott; 1994; p. 193)

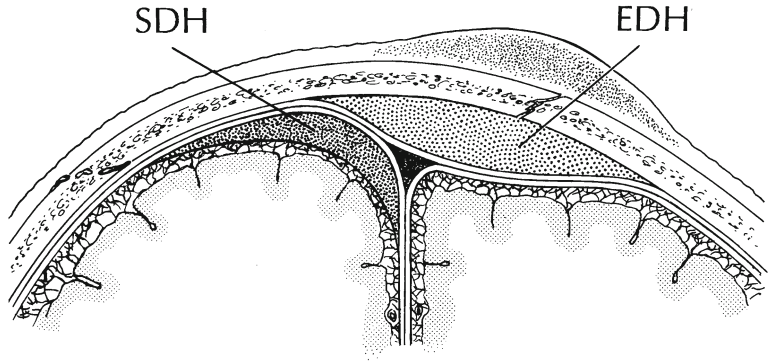


**Fig. 2.5** Coronal diagram of the EDH and SDH. The EDH is located above the outer dural layer (i.e., the periosteum), and the SDH is located beneath the inner (meningeal) dural layer. The EDH does not cross sutures. The SDH does not directly cross the falx or the tentorium. (Reprinted with permission from Gean AD. Imaging of head trauma. Philadelphia, PA: Williams & Wilkins-Lippincott; 1994, p. 76)

## Subdural Hematoma

The *subdural hematoma* (SDH) occurs above the arachnoid and beneath the inner meningeal layer of the dura (Fig. 2.5). Because the dura and arachnoid are not firmly attached, the SDH is frequently seen layering along the entire hemispheric convexity from the anterior falx to the posterior falx. The SDH usually develops from

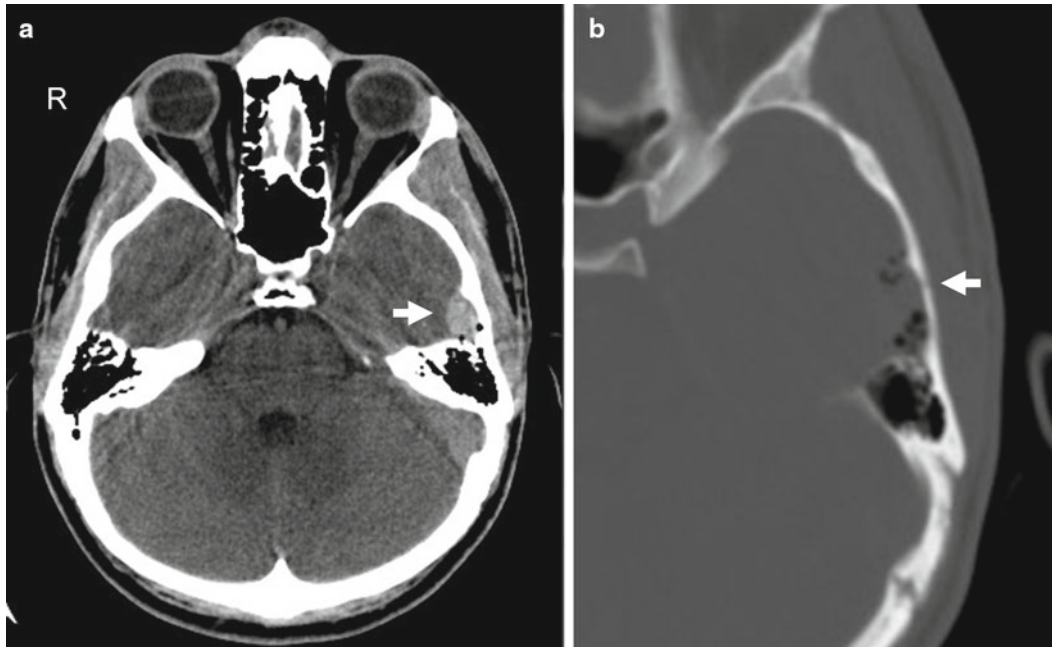


**Fig. 2.6** Acute EDH. (**a**) Non-contrast axial CT shows a characteristic hyperdense, homogeneous, biconvex left temporal extra-axial collection (*arrow*). (**b**) An adjacent axial CT slice, displayed in bone window, reveals associated pneumocephalus and a linear non-displaced fracture of the left temporal bone (*arrow*)

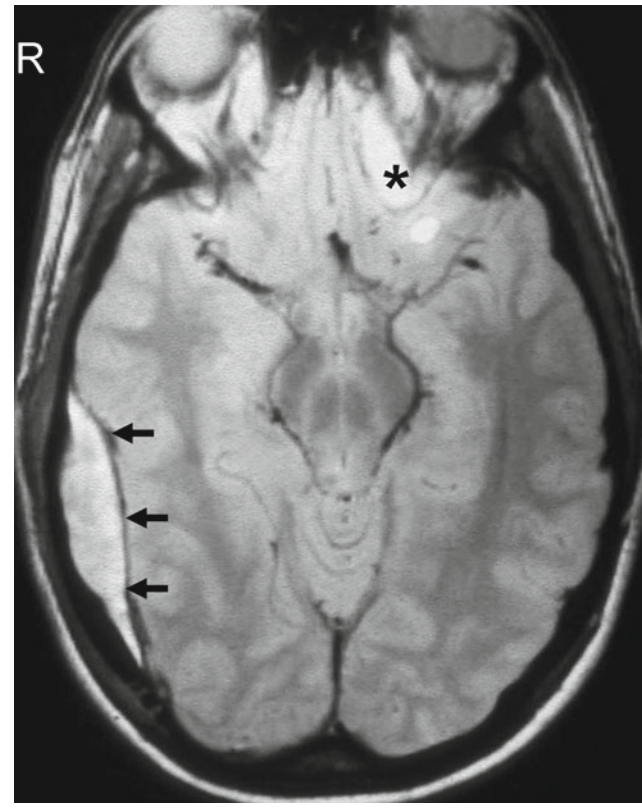


**Fig. 2.7** Subacute EDH on MRI. Proton density-weighted axial MR image shows a thin dark line (*horizontal arrows*) displaced by the extra-axial collection, indicating the epidural location of the hematoma. A contrecoup left orbitofrontal contusion is also evident (*asterisk*). (Reprinted with permission from Gean AD. Imaging of head trauma. Philadelphia, PA: Williams & Wilkins-Lippincott; 1994, p. 119)

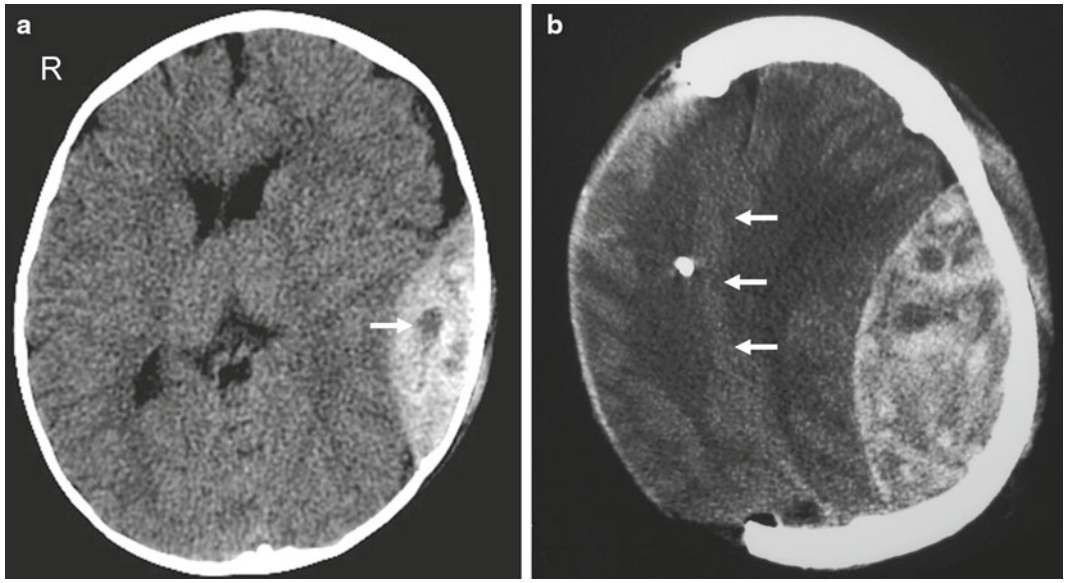


**Fig. 2.8** EDH "swirl sign". (**a**) Axial CT image shows low attenuation areas (*arrow*) within a left frontotemporal heterogenous acute EDH. The heterogeneous density within this EDH is secondary to mixing of hyperacute (low attenuation) with acute (high attenuation) blood. (**b**) Axial CT image from another patient, performed following decompressive craniectomy, demonstrates right external herniation, left-to-right subfalcine herniation (*arrows*), and formation of a contralateral, heterogenous EDH

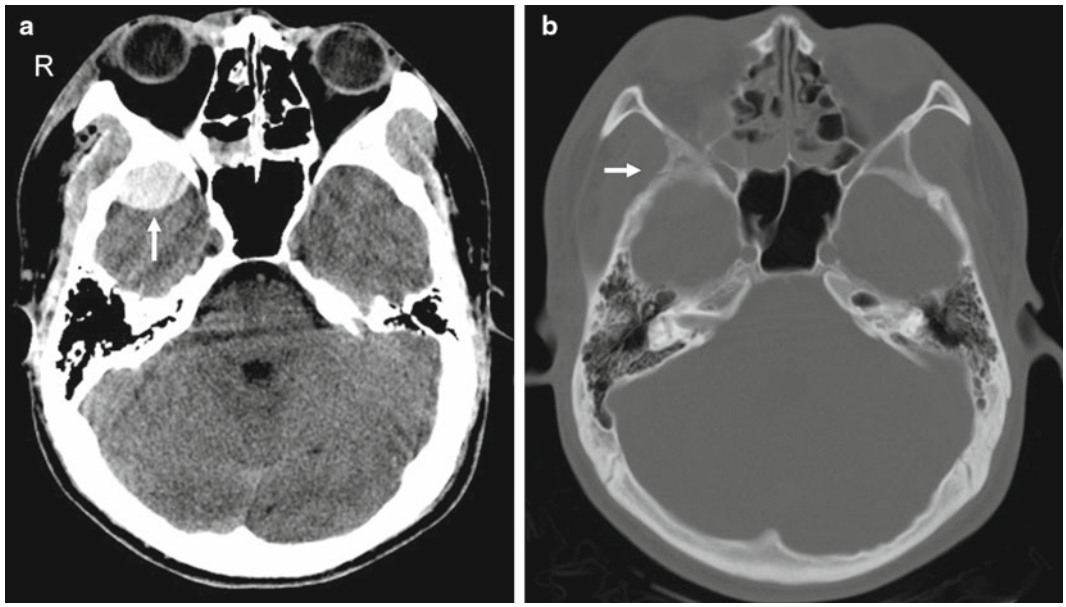


**Fig. 2.9** Venous EDH. (**a**) Axial CT image shows a biconvex, homogeneous, high attenuation extra-axial collection within the right middle cranial fossa (*vertical arrow*). (**b**) CT image displayed in "bone window" reveals a fracture of the right greater sphenoid wing (*horizontal arrow*). The location suggests that the hematoma is due to disruption of the sphenoparietal sinus. (Reprinted with permission from Le TH and Gean AD. Neuroimaging of traumatic brain injury. Mt Sinai J Med. 2009;76:145–162)

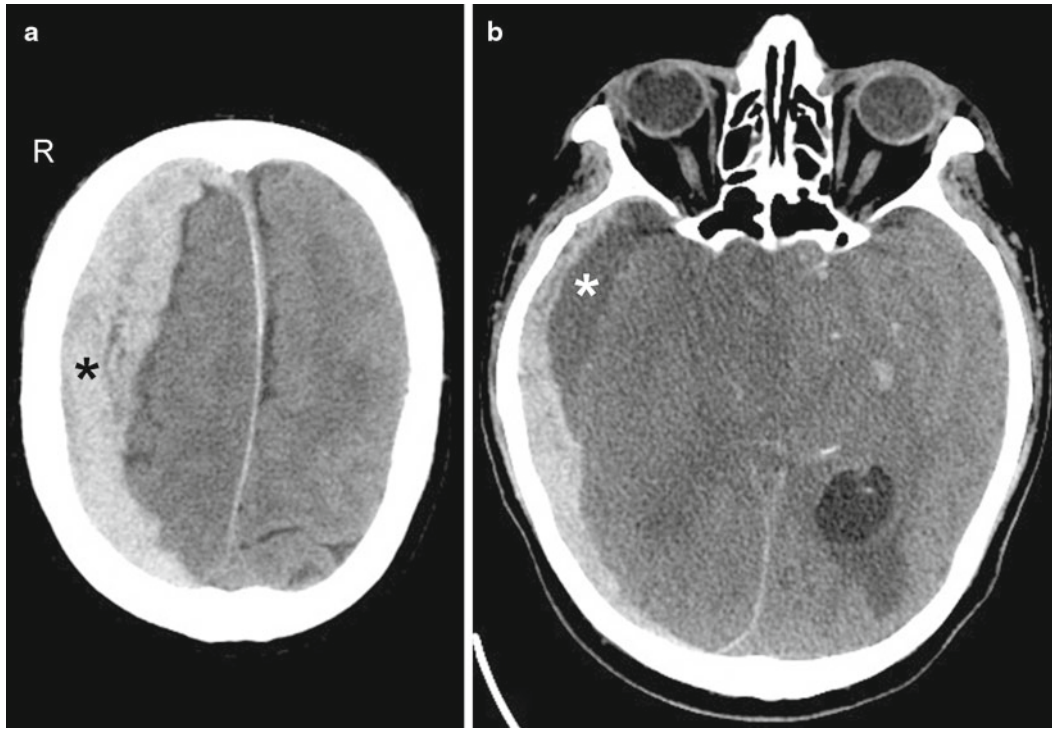


**Fig. 2.10** SDH. (**a**) Non-contrast axial CT image demonstrates a right hyperdense, holohemispheric extra-axial collection (*asterisk*), causing mass effect and sulcal effacement of the right cerebral hemisphere. There is also mild right-to-left subfacine herniation. (**b**) Non-contrast axial CT image shows a low-density area (*asterisk*) corresponding to a chronic SDH component within an acute right temporal SDH. There is associated loss of gray-white matter differentiation and diffuse decrease in attenuation of the right temporal lobe and midbrain due to cerebral edema and ischemia. There is effacement of the cisterns. Multiple foci of small hemorrhages within the left temporal lobe indicate axonal injuries. There is also dilatation of the occipital horn of the left ventricle

laceration or disruption of bridging cortical veins, especially during sudden head deceleration. Disruption of bridging cortical veins can also occur with rapid decompression of obstructive hydrocephalus, when the brain surface recedes from the dura quicker than the brain parenchyma can re-expand after being compressed by the distended ventricles. SDH can also arise from injury to pial vessels, pacchionian granulations, or penetrating branches of superficial cerebral arteries. The incidence of SDH is higher in the elderly because the increase in extra-axial space from cerebral atrophy allows for increased motion between the brain parenchyma and the calvarium.

Most SDHs are supratentorial and located over the convexity, especially the parietal region. They are frequently seen along the falx and tentorium. Unlike EDHs, SDHs frequently occur at the contrecoup site. Because the SDH is often associated with parenchymal injury, the degree of mass effect may appear more extensive than the size of the SDH blood collection.

On CT, the acute SDH appears as a hyperdense, homogenous, and crescent-shaped collection (Fig. 2.10a). Compared to normal brain (20–30 HU), the density (attenuation) of an acute SDH (50–60 HU) is higher because of clot retraction. The density of the SDH will progressively decrease as protein degradation occurs. Rebleeding during evolution of a SDH appears as a heterogeneous mixture of fresh blood and partially liquefied hematoma (Fig. 2.10b). A sediment level or "*hematocrit effect*" may be seen from either rebleeding or in patients with clotting disorders.

Between 1 and 3 weeks following injury, an isodense SDH phase occurs. The timing depends


**Fig. 2.11** Isodense subacute SDH. Non-contrast axial CT image shows bilateral isodense SDHs. During the transition from acute to chronic SDH, an isodense phase occurs. At this stage, the SDH (*asterisk*) can be difficult to differentiate from the adjacent brain parenchyma. Note displacement of the gray-white matter junction from the inner table of the skull (the "*thick gray matter mantle*" sign)

on the patient's hematocrit level, clotting capability, and presence or absence of re-bleeding. During this subacute period, a small thin convexity isodense SDH can be difficult to identify on CT (Fig. 2.11). Imaging findings such as sulcal effacement, effacement or distortion of the white matter (white matter "*buckling*"), abnormal separation of the gray-white matter junction from the inner table of the skull ("*thick gray matter mantle*"), distortion of the venticles, and midline shift are indirect signs that can improve detection of isodense SDHs.

The chronic SDH has density similar to, but slightly higher than, cerebrospinal fluid on CT (Fig. 2.12). It may be difficult to distinguish from prominent subarachnoid space in patients with cerebral atrophy. In these patients, a contrast-enchanced CT can improve detection of the chronic SDH by demonstrating an enhancing capsule or displaced cortical veins. Over time, activated fibroblasts and blood vessels from the dura organize within the SDH. The fragile penetrating vessels are prone to bleeding, which can lead to the dreaded "*chronic recurrent*" SDH. The chronic recurrent SDH may not be crescentic in shape because of dural adhesions, and it is typically heterogeneous with multiple internal septations, loculations, and fluid levels (Fig. 2.13f).

The MRI signal characteristics of the SDH vary depending on the age of the blood products (Gomori et al. 1985; Fobben et al. 1989). The acute SDH is isointense to brain on T1-weighted images and hypointense on T2-weighted images. During the subacute phase, when the SDH is isodense on non-contrast CT images, the SDH has a high signal intensity on T1-weighted images due to the presence of methemoglobin (Fig. 2.13a). The chronic SDH appears hypointense on T1-weighted and hyperintense on T2-weighted images relative to normal brain. The signal intensity of the chronic SDH is typically slightly higher than CSF signal intensity on T1- and T2-weighted and FLAIR images (Fig. 2.13b). The lack of beam-hardening artifact and the capability of multiplanar imaging make MRI particularly useful in identifying small convexity and vertex hematomas that may not be readily recognized on axial CT.


**Fig. 2.12** Chronic SDH. Non-contrast axial CT image demonstrates bilateral low-density collections (*asterisk*) due to chronic SDHs. The chronic SDH has attenuation slightly higher than CSF

### Subarchnoid Hemorrhage

Traumatic *subarachnoid hemorrhage* (SAH) can develop from disruption of small pial vessels due to skull fracture or brain motion, from contiguous extension into the subarachnoid space by a contusion or a hematoma, or from spread of intraventricular hemorrhage via the fourth ventricular outlet foramina. Common sites for traumatic SAH include the sylvian fissure, the interpeduncular cistern, and the high convexity. The greatest accumulation of SAH tends to occur on the contrecoup side.

On CT, acute SAH appears as areas of high density that conform to the morphology of the cerebral sulci and cisterns (Fig. 2.14). SAH along the convexity or tentorium can be difficult to differentiate from a SDH. A useful distinguishing clue is the extension of the SAH into adjacent sulci. Occasionally, "effacement" of the sulci due to the presence of intra-sulcal SAH is the only imaging clue of the presence of SAH.

Acute SAH is more difficult to detect on conventional T1- and T2-weighted MRI than on CT because intracellular oxyhemoglobin and/or deoxyhemoglobin is isointense to brain parenchyma. However, FLAIR is potentially more sensitive than CT, especially when at a volume of at least 1–2 mL is present (Woodcock et al. 2001). Subacute SAH, when the blood is isointense to CSF on CT, is better recognized on MRI because of the high signal intensity of extracellular methemoglobin. SAH more than 1-week old would be difficult, if not impossible, to detect on CT. Chronic SAH is better detected on MRI and is invisible on CT. Old blood products, such as hemosiderin in the subarachnoid space ("superficial hemosiderosis"), are best detected on SWI and GRE T2*-weighted images (Fig. 2.15) and appear as areas of decreased signal intensity.

### Intraventricular Hemorrhage

Traumatic *intraventricular hemorrhage* (IVH) can result from rotationally-induced tearing of subependymal veins along the surface of the ventricles, from contiguous extension of a parenchymal

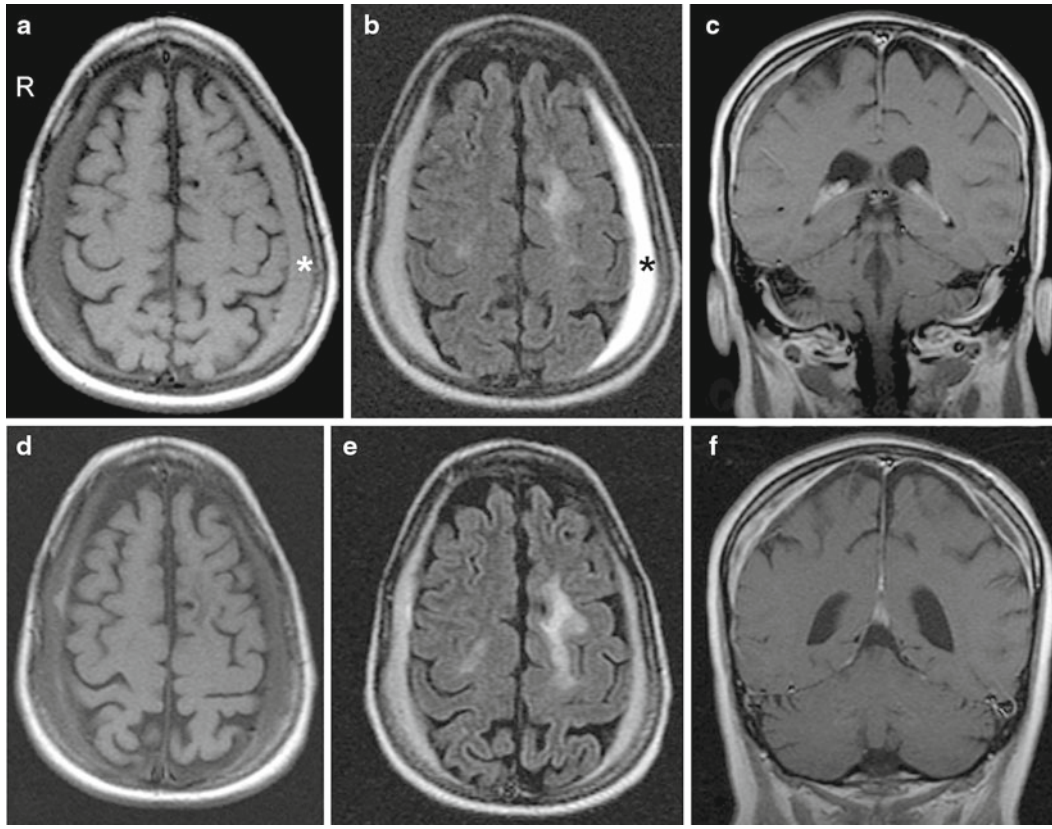


**Fig. 2.13** MRI of SDH. (**a**) Axial T1-weighted MR image, performed on a 0.7 T open MRI, reveals bilateral holohemispheric SDHs. The subacute left SDH has signal intensity relatively higher than adjacent parenchyma due to the presence of methemoglobin. (**b**) The corresponding FLAIR image shows that the subacute left SDH is quite intense. The chronic right SDH has signal intensity higher than the suppressed CSF signal. (**c**) The SDHs also have enhancing capsules, as seen on the coronal T1-weighted post-contrast image. (**d**) Axial T1-weighted image, performed 2 months later, shows evolution of the left SDH, which is now low in intensity. (**e**) Both SDHs are now of similar intensity on FLAIR. (**f**) Coronal T1-weighted post-contrast image shows heterogenous enhancement within the right SDH due to the presence of activated fibroblasts and blood vessels from the dura organized within the SDH

hematoma into the ventricular system, or from retrograde flow of SAH into the ventricles (Fig. 2.14). Direct penetrating wounds can also cause IVH. Patients with IVH are at risk for developing non-communicating hydrocephalus from obstruction of the aqueduct due to ependymal proliferation ("ependymitis") and/or communicating hydrocephalus from obstructive scarring of the arachnoid villi.

On CT, acute IVH typically appears as a hyperdense collection layering dependently within the ventricular system, forming a CSF-blood fluid level (Fig. 2.14). Sometimes, a tiny collection of increased density layering posteriorly in one occipital horn may be the only clue to IVH. Occasionally, the IVH appears "tumefactive" or "mass-like" as a cast within the ventricle.

## Primary Intra-Axial Injury

### Diffuse Axonal Injury

Traumatic *axonal injury* refers to white matter damage arising from shear-strain deformation of brain tissue following rotational acceleration and deceleration injury. When the skull is rapidly rotated, axial stretching, separation, and disruption of the white matter fibers occur because the non-rigid brain and brainstem lag behind. *Diffuse axonal injury* (DAI) indicates extensive injury to


**Fig. 2.14** SAH and IVH. Non-contrast axial CT image demonstrates bilateral high attenuation collections conforming to the sylvian sulci due to acute SAH. The greatest collection of SAH is within the right sylvian sulcus (*horizontal arrows*). Small high-density collection layering within the occipital horn of the right lateral ventricle is compatible with acute IVH (*vertical arrow*)

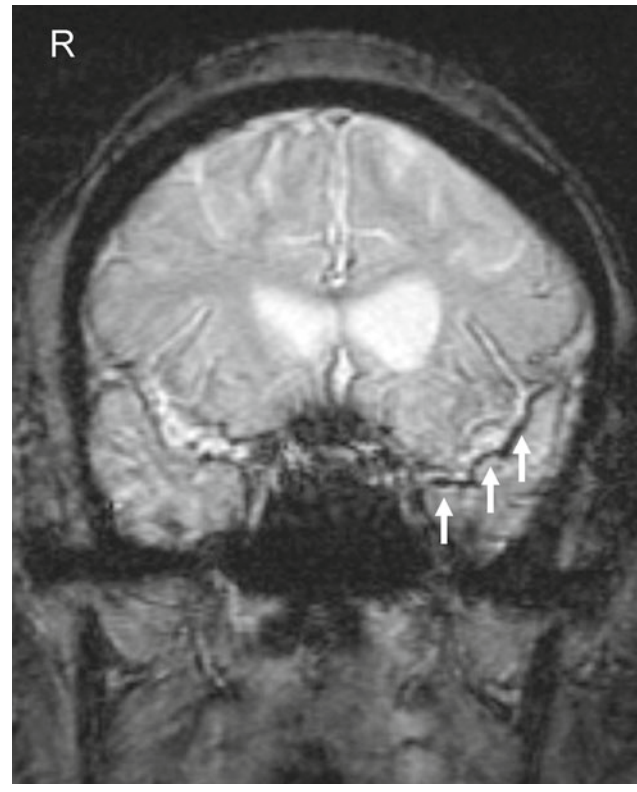


**Fig. 2.15** Chronic SAH on GRE MRI. Coronal GRE T2*-weighted image demonstrates bilateral decrease in signal within the temporal sulci, with the greatest accumulation within the left sylvian sulcus (*arrow*) due to hemosiderin deposits (superficial siderosis)

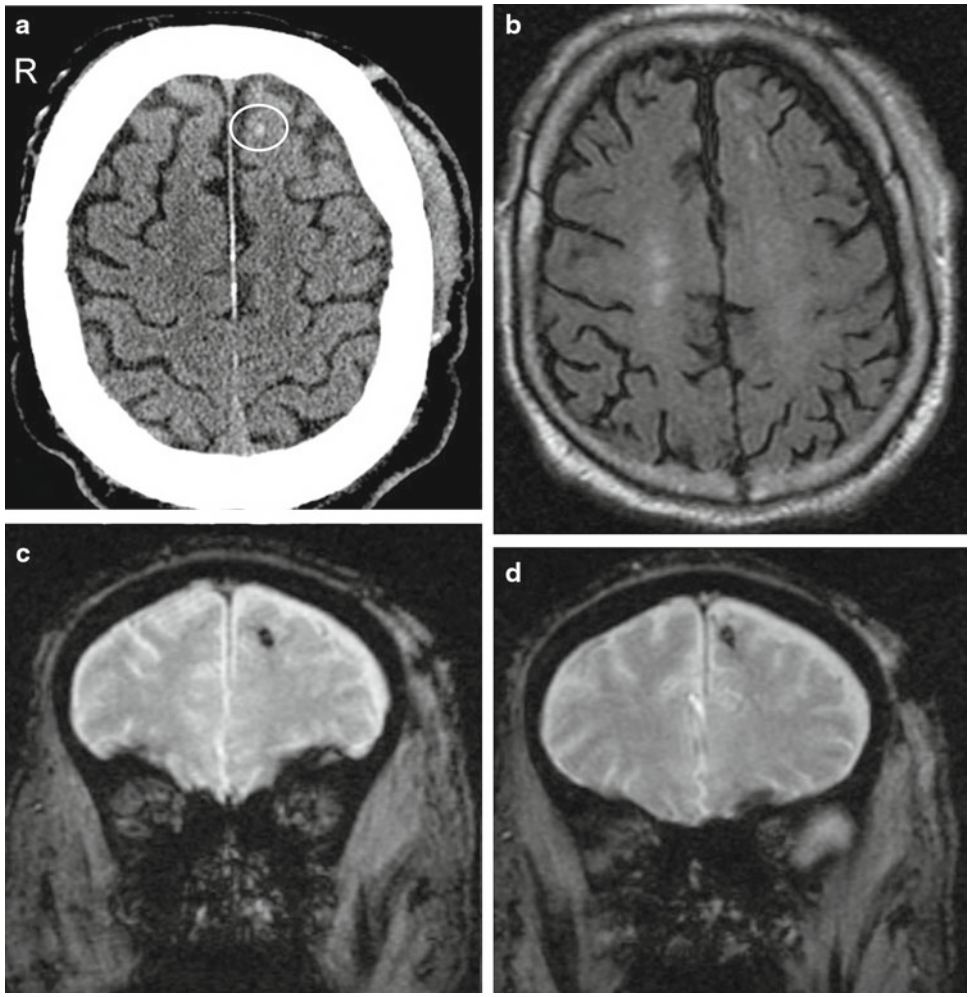


**Fig. 2.16** Grade I DAI. (**a**) Non-contrast axial CT image reveals a small high-density focus within the subcortical white matter of the left frontal lobe, compatible with hemorrhagic shear injury. (**b**) Follow-up axial FLAIR image demonstrates a corroborated subcortical focus of T2 hyperintensity. There is an additional left frontal subcortical focus of FLAIR hyperintensity that is not visible on the CT image. Nonspecific T2 signal abnormality within the bilateral centrum semiovale is also noted. (**c** and **d**) Coronal GRE T2*-weighted images show corresponding foci of hemorrhagic shear injury within the left frontal lobe

the white matter and occurs in up to 50% of severe head trauma cases (Jennett et al. 2001). DAI is of special interest because it is believed to be responsible for the majority of unexplained cognitive deficits following head trauma. DAI is under diagnosed by conventional imaging techniques (Inglese et al. 2005; Mittl et al. 1994).

DAI tends to occur in three classic regions ("*shearing injury triad*"): the lobar white matter, the corpus callosum, and the dorsolateral quadrant of the rostal brainstem adjacent to the superior cerebellar peduncle. The location of DAI generally correlates with the severity of the trauma (Gennarelli et al. 1982). Mild (Grade I) DAI typically involves only the peripheral gray–white junction of the lobar white matter, commonly the parasagittal regions of the frontal lobes and the temporal stem (Fig. 2.16). With moderate (Grade II) DAI, the corpus callosum, particularly the posterior body and splenium, in addition to the lobar white matter, is involved (Fig. 2.17). In severe (Grade III) DAI, the dorsolateral midbrain, in addition to the lobar white matter and corpus callosum, is affected.

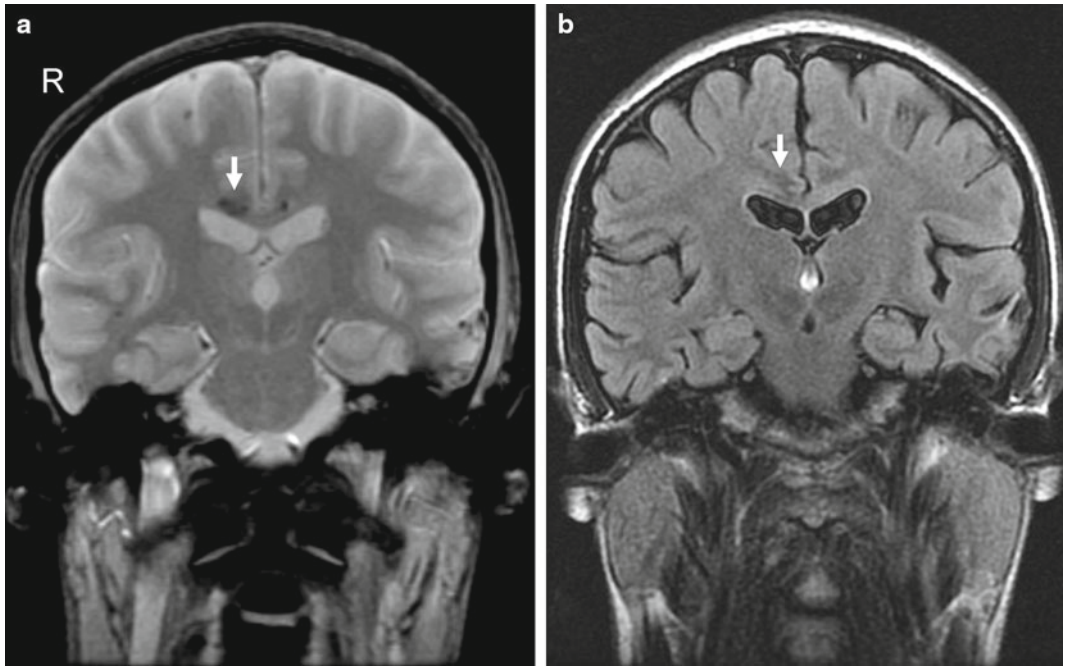


**Fig. 2.17** Grade II DAI. (**a**) Coronal GRE T2*-weighted image demonstrates multiple foci of low signal (hemorrhages) within the peripheral gray-white junction of the bilateral temporal and right frontal lobes. Abnormal foci of low signal are also seen within the corpus callosum (*arrow*). (**b**) The callosal injury is low in signal intensity on FLAIR (*arrow*) and is not as easily detectable

On CT, DAI lesions appear as small high attenuation foci (shear hemorrhages) at the gray–white junction of the cerebral hemispheres (Fig. 2.16a), corpus callosum, and the dorsolateral midbrain, depending on the severity of the trauma. Because of its higher sensitivity to blood products, GRE T2*-weighted MRI reveals more hemorrhagic DAI lesions than CT (Mittl et al. 1994). Even so, detection of hemorrhagic shear alone does not fully describe the extent of DAI (Adams et al. 1991). FLAIR MRI can identify additional non-hemorrhagic foci of DAI but still underestimates the true extent of the diffuse white matter damage (Ashikaga et al. 1997). Non-hemorrhagic acute DAI lesions appear as multiple small foci of increased signal on T2-weighted images and decreased signal on T1-weighted images. On DWI, acute DAI can show reduced ADC (Fig. 2.18) and reduced FA. In subacute DAI, intracellular methemoglobin from petechial hemorrhage appears as an area of central hypointensity on T2-weighted images and hyperintensity on T1-weighted images. The conspicuity of DAI on MRI eventually diminishes as the damaged axons degenerate and the edema resolves. Chronic DAI imaging findings include nonspecific atrophy, gliosis, wallerian degeneration, and hemosiderin staining. The FA is generally reduced in chronic DAI.

MRI is superior to CT in detecting axonal injuries, especially when susceptibility-weighted sequences and higher field strength magnets (3T) are used (Lee et al. 2008). Yet even with MRI, the incidence of DAI is still thought to be underestimated. Advanced MR imaging methods, such as DTI with 3D tractography (Fig. 2.18), have shown potential in improving the detection of white matter injury in both acute and chronic DAI (Arfanakis et al. 2002; Huisman et al. 2003; Le et al. 2005). MRS and MTI can also offer additional prognostic value in DAI (Sinson et al. 2001).

### Cortical Contusion

The *cortical contusion* is a hemorrhagic parenchymal injury ("brain bruise") involving predominantly the superficial gray matter with relative

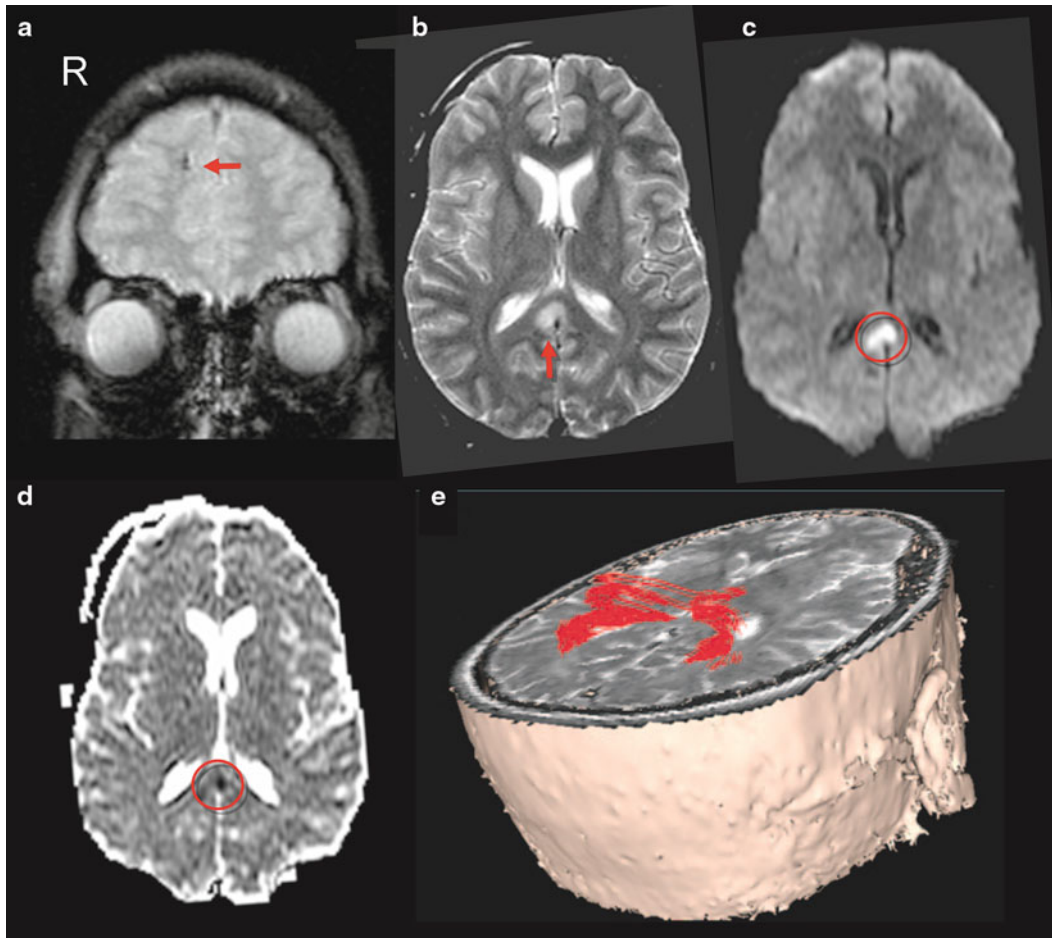


**Fig. 2.18** Grade II DAI (Acute) on DWI. (**a**) Coronal GRE T2*-weighted MR image reveals a focus of dark signal (*arrow*) at the gray-white junction of the right frontal lobe consistent with hemorrhagic shearing injury. (**b**) T2-weighted image shows abnormal bright signal within the splenium (*arrow*) of the corpus callosum. (**c**) Diffusion-weighted image and (**d**) corresponding ADC map show restricted diffusion in the same area (*circle*). (**e**) 3D color tractography demonstrates disruption of the commissural fibers at the posterior inferior margin of the splenium of the corpus callosum. (Reprinted with permission from Le TH, Mukherjee P, Henry RG, et al. Diffusion tensor imaging with three-dimensional fiber tractography of traumatic axonal shearing injury: an imaging correlate for the posterior callosal "disconnection" syndrome: case report. Neurosurgery. Jan 2005;56(1):189)

sparing of the underlying white matter. Regions of the brain that are in close contact with the rough inner surfaces of the skull are typically affected. Regions within the temporal lobes (above the petrous bone and posterior to the greater sphenoid wing) and the frontal lobes (above the cribriform plate, orbital roof, and lesser sphenoid wing) are the most commonly affected. Contusions are also common subjacent to depressed skull fractures. Contusions along the parasagittal convexity are less common. The cerebellum is infrequently involved (Gentry 1996).

On CT, hemorrhagic contusions appear as mottled areas of high density within the superficial gray matter (Fig. 2.19). They may be surrounded by larger areas of low density from associated vasogenic edema. As the contusion evolves, a "salt and pepper" pattern of mixed areas of hypodensity and hyperdensity is characteristic. Non-hemorrhagic contusions appear as

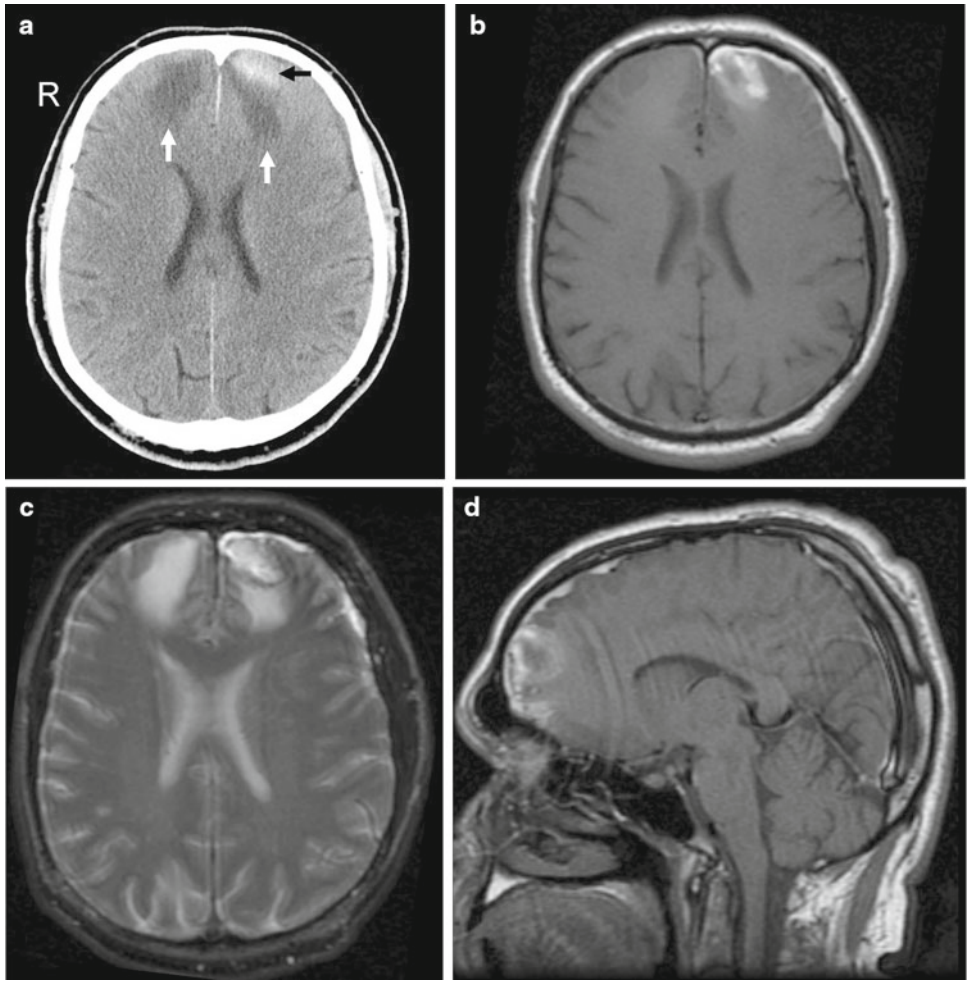


**Fig. 2.19** Contusion on CT and MRI. (**a**) Axial CT shows an amorphous high-density area within the left orbitofrontal lobe consistent with an acute contusion (*horizontal arrow*). Bilateral frontal lobe low attenuation (*vertical arrow*) represents either vasogenic edema and/or non-hemorrhagic contusion. (**b**) Follow-up axial T1-weighted MR image shows corresponding high signal due to the presence of methemoglobin. A thin left SDH is also noted. (**c**) Axial T2-weighted image shows the left hemorrhagic contusion of mixed high and dark signal, while the bilateral frontal non-hemorrhagic contusions versus vasogenic edema are more homogenous in appearance. (**d**) Sagittal T1-weighted MR image displays an area of left inferior frontal surface contusion, in addition to the more superior contusion and the left SDH seen in (**b**)

low density areas and can be difficult to detect initially until the development of sufficient edema. Due to its superficial location, the cortical contusion can be difficult to detect on CT, especially in the presence of beam hardening streak artifacts.

MRI can provide better delineation of contusions than CT since the skull does not distort the MR images. In addition, different MR techniques allow for emphasis on blood products at different ages (Hesselink et al. 1988). On MRI, contusions appear as ill-defined areas of variable signal intensity on both T1- and T2-weighted images, depending on the age of the lesions. Since contusions mainly involve the surface of the brain, they may have a "gyral" morphology. An old contusion commonly evolves into a wedge-shaped area of peripheral encephalomalacia with the broad base facing the skull. Therefore, it can mimic an old ischemic infarction.

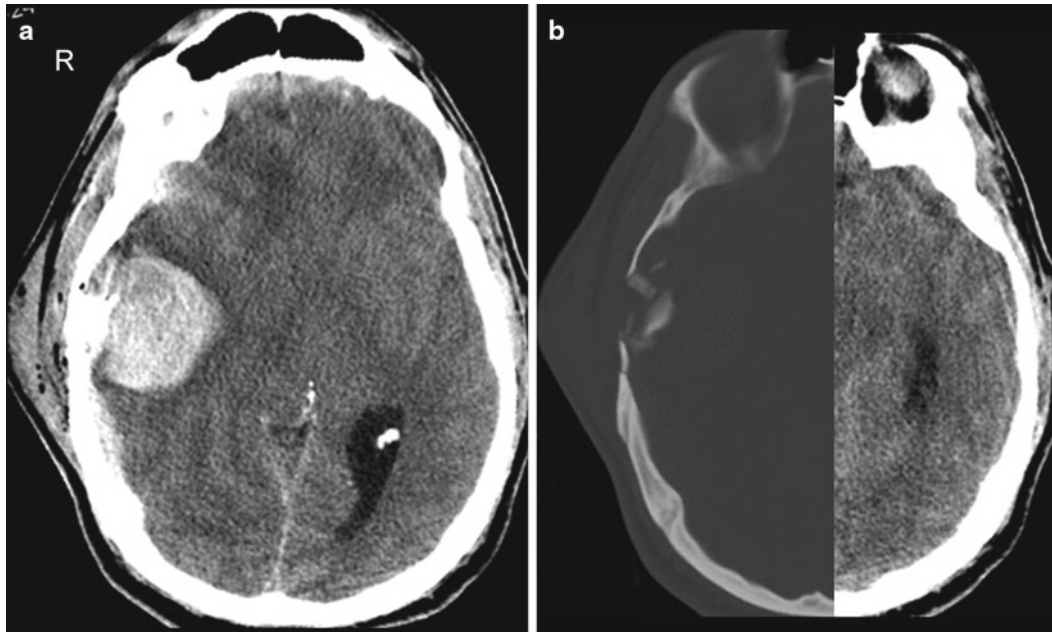


**Fig. 2.20** ICH and skull fractures. (**a**) Non-contrast axial CT image, from a patient who sustained a snowboarding accident, shows a large round right posterior frontal intra-axial high attenuation mass due to an acute intracerebral hematoma. There is marked adjacent scalp soft-tissue swelling. (**b**) CT image, displayed in bone window, reveals a comminuted depressed skull fracture

### Intracerebral Hematoma

The *intracerebral hematoma* (ICH) can develop from microcavitation or shear-induced hemorrhage of small intraparenchymal blood vessels or from expansion and coalescence of adjacent cortical contusions. In essence, the latter mechanism suggests that contusion and hematoma can be the same entity. Like contusions, ICHs frequently involve the frontotemporal white matter. Intracerebral hematomas are often associated with skull fractures and other primary intracranial injuries, including contusions and DAI, especially in patients who are unconscious at the time of injury. Several characteristic differences between the contusion and the hematoma should be noted. The ICH is usually more well defined and tends to have less surrounding edema than the cortical contusion. Intracerebral hematomas are often located deeper in the brain than cortical contusions. The intracerebral hematoma is the most common cause of clinical deterioration in patients who have experienced a lucid interval after the initial injury (Reilly et al. 1975). Delayed hemorrhage is a common cause of clinical deterioration during the first several days after head trauma (Soloniuk et al. 1986).

On CT, the acute intracerebral hematoma appears as a rounded hyperdense mass (Fig. 2.20). As the hematoma evolves, a low density rim, due to edema and pressure necrosis, can be observed. Contrast ring-enhancement can be seen within a subacute hematoma because of the proliferation of new capillaries lacking a complete blood–brain barrier. The enhancing subacute hematoma can be difficult, if not impossible, to differentiate from an abscess, infarct, or neoplasm without accurate clinical history or novel imaging methods such as MRS or DWI. The imaging findings of the chronic intracerebral hematoma are nonspecific, but involvement of the orbitofrontal and anteroinferior temporal lobes is typical.

On occasion, approximately 1–4 days following the onset of the initial trauma, delayed intracerebral hematomas can occur in areas that

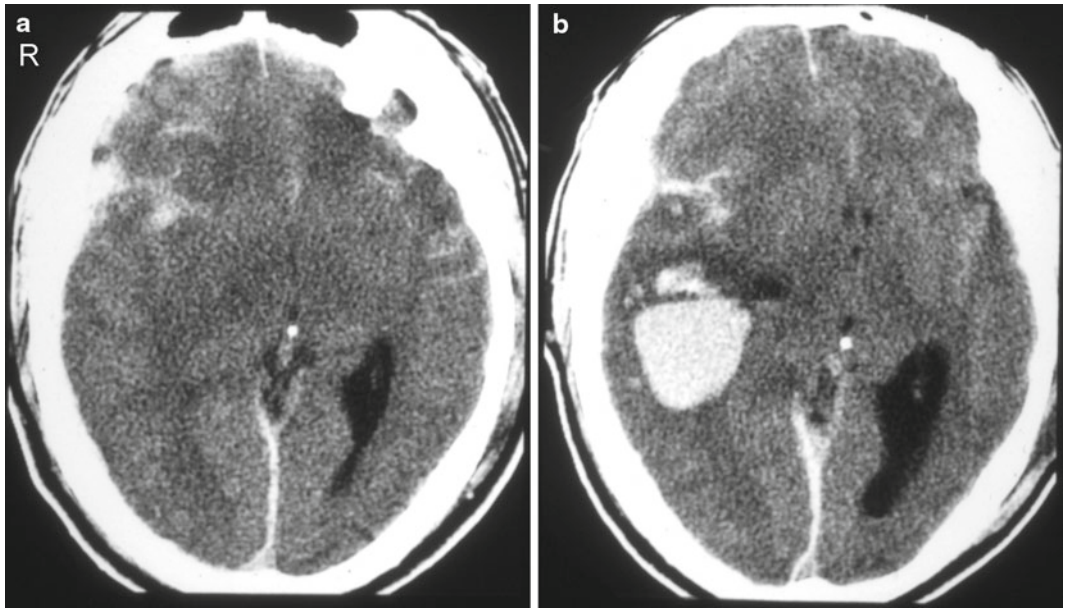


**Fig. 2.21** "Delayed" intracerebral hematoma. (**a**) Noncontrast axial CT scan on admission demonstrates bilateral frontotemporal subarachnoid hemorrhages, right-to-left midline shift, and effacement of the right occipital horn, but without focal mass lesion. (**b**) The 4-h follow-up study reveals interval development of a large right temporal hematoma in the area of prior mass effect. (Reprinted with permission from Gean AD. Imaging of head trauma. Philadelphia, PA: Williams & Wilkins-Lippincott; 1994, p. 185)

previously demonstrated focal contusions on CT or MRI (Lipper et al. 1979; Nanassis et al. 1989). These delayed hematomas tend to occur in multiple lobar locations and are associated with a poor prognosis (Fig. 2.21). The proposed pathogenesis is due to reperfusion hemorrhage secondary to vasospasm with subsequent vasodilation or hypotension with subsequent hypertension, and may be further exacerbated by an underlying coagulopathy.

### Encephalomalacia

*Encephalomalacia* is a nonspecific imaging finding but can develop in areas from either primary or secondary injury. It appears as a focal well-defined area of tissue loss with compensatory dilatation of the ipsilateral ventricle and sulci, and/or presence of old blood products. Macrocystic encephalomalacia follows CSF signal intensity on both CT and MR. Microcystic encephalomalacia appears as low signal intensity on T1-weighted MR images and high intensity on T2-weighted and FLAIR images.

## Vascular Injury

Vascular injuries can lead to both intra- and extra-axial injuries, including hematomas and SAH. Traumatic vascular injuries can result from blunt or penetrating trauma and include arterial dissection, pseudoaneurysm, and arteriovenous fistula. Vascular injuries are often related to skull base fractures. The internal carotid artery is the most commonly affected vessel. The injury usually occurs at sites of relative fixation, where the internal carotid artery enters the carotid canal at the base of the petrous bone and at its exit from the cavernous sinus beneath the anterior clinoid process.

### Arterial Dissection

A traumatic *arterial dissection* develops when there is incomplete disruption of the vessel wall with formation of a subintimal or intramural hematoma. The dissection is often best detected with T1-weighted MR images with fat suppression where the hematoma appears as a bright "crescent sign" (Fig. 2.22a). The affected vessel

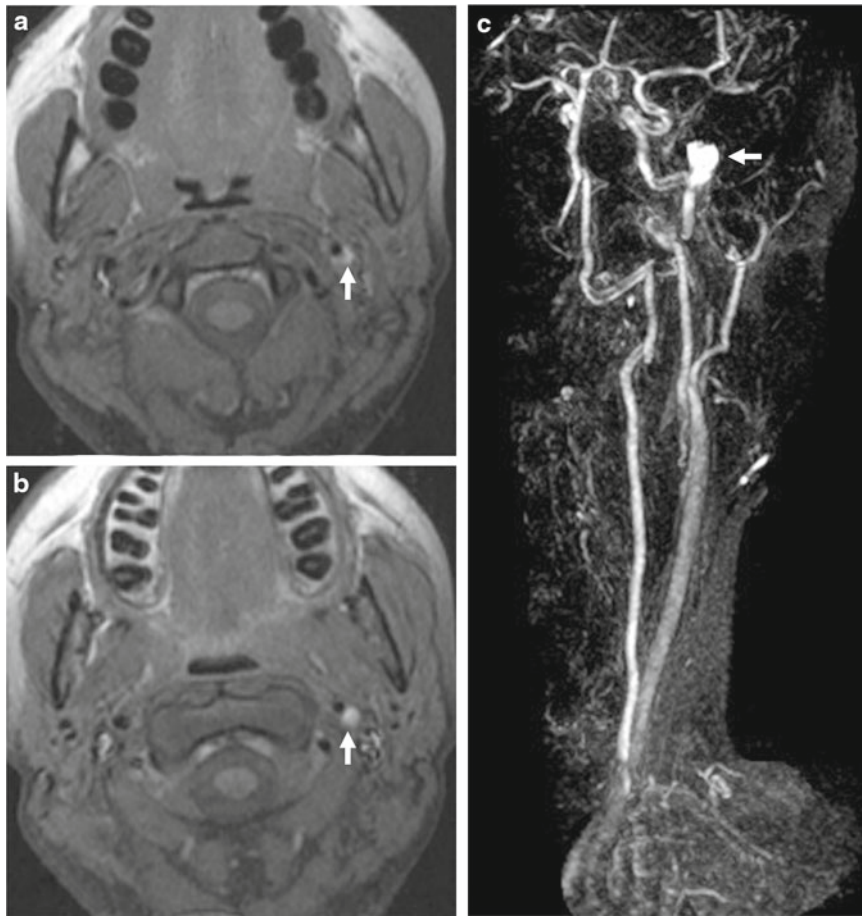


**Fig. 2.22** Arterial dissection and pseudoaneurysm. (**a**) Axial T1-weighted with fat suppression image demonstrates a left common carotid artery high intensity rim due to an intramural hematoma from a focal dissection (*arrow*). (**b**) Image superior to the focal dissection shows a round extra-luminal high-density focus (*arrow*). (**c**) MRA of the neck shows a lobular "mass" protruding from the vessel, compatible with a pseudoaneurysm (*arrow*)

may appear irregular with relatively smaller caliber. Absence of the normal vascular flow void and abnormal flow-related enhancement secondary to slow flow, intraluminal thrombus, or vessel occlusion may be identified on MRI and MRA. A watershed and/or embolic parenchymal infarction (secondary injury) supplied by the injured vessel may occur.

Conventional catheter angiography has been traditionally considered to be the gold standard for confirmation and delineation of the vascular dissection, and it can also reveal associated vasospasm and pseudoaneurysm. However, MR angiography and CT angiography are increasing being used as noninvasive screening tools in patients with suspected vascular injury. In addition, because catheter angiography only demonstrates the caliber of the patent lumen, MR and CTA can identify a dissected vessel that may appear "normal" on catheter angiography. MR and CT are equally sensitive for the detection of intramural hematoma and subintimal flap, but CTA is more sensitive in depicting vertebral artery pseudoaneurysms (Vertinsky et al. 2008).

### Pseudoaneurysm

*Pseudoaneurysms* are rare in adults but account for 11% of all pediatric aneurysms, although the overall incidence of aneurysms in pediatrics is relatively lower than in adults (Hardwood-Nash

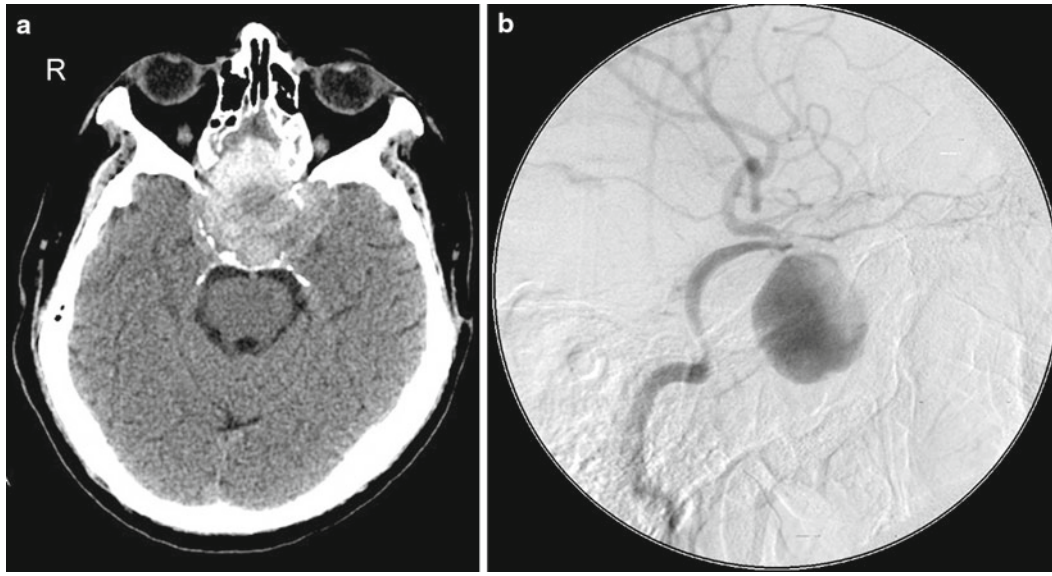


**Fig. 2.23** Giant pseudoaneurysm. (**a**) Non-contrast axial CT image shows a large mixed low and high attenuation suprasellar mass. (**b**) Corresponding catheter cerebral angiogram from a selective left ICA injection shows a large mass partially filled with contrast arising from the left ICA, compatible with a partially thrombosed pseudoaneurysm

and Fritz 1976; Dubey et al. 2008). Typically, the wall of the pseudoaneurysm is actually an encapsulated hematoma in communication with the artery. On occasion, the adventitia may still be intact. Nevertheless, the wall of the pseudoaneurysm provides little support, and hence it has a propensity to hemorrhage. The pseudoaneurysm can also arises from a focal dissection ("*dissecting pseudoaneurysm*") (Fig. 2.22b, c). On imaging, the pseudoaneurysm frequently has an irregular contour and a wide neck. Thrombosis within the pseudoaneurysm manifests as a rounded mass with concentric laminated rings of heterogeneous signal intensity, consistent with thrombus in various stages of evolution (Fig. 2.23). The size of a partially thrombosed pseudoaneurysm is underestimated on conventional angiography because the angiogram only depicts the patent portion of the lesion. MRI and CT can better reveal the true extent of a partially thrombosed pseudoaneurysm than angiography. In the absence of thrombosis or turbulent flow, the pseudoaneurysm appears as a round area of signal void on both T1- and T2-weighted images. Pulsation within the pseudoaneurysm shows phase artifacts on MRI, a helpful imaging clue to the presence of a vascular lesion.

### Arteriovenous Fistula

The traumatic *arteriovenous fistula* is a direct communication between an artery and a vein. The *carotid cavernous fistula* (CCF) is a direct communication between the cavernous portion of the internal carotid artery and the adjacent cavernous sinus venous plexus (Fig. 2.24). Traumatic CCF typically results from a full-thickness arterial injury, and can occur following either blunt or penetrating TBI. A CCF is also thought to be preceded by a traumatic pseudoaneurysm of the internal carotid artery. Classic imaging features of the CCF include engorgement of the cavernous and petrosal sinuses and a dilated tortuous ipsilateral superior ophthalmic vein. When the superior ophthalmic vein exceeds 4 mm in diameter, a CCF should be suspected. Other imaging findings include enlarged extraocular muscles, proptosis, retrobulbar fat stranding, pre-septal soft tissue swelling, and an ipsilateral convex cavernous sinus. These findings may even be bilateral and symmetric because venous channels

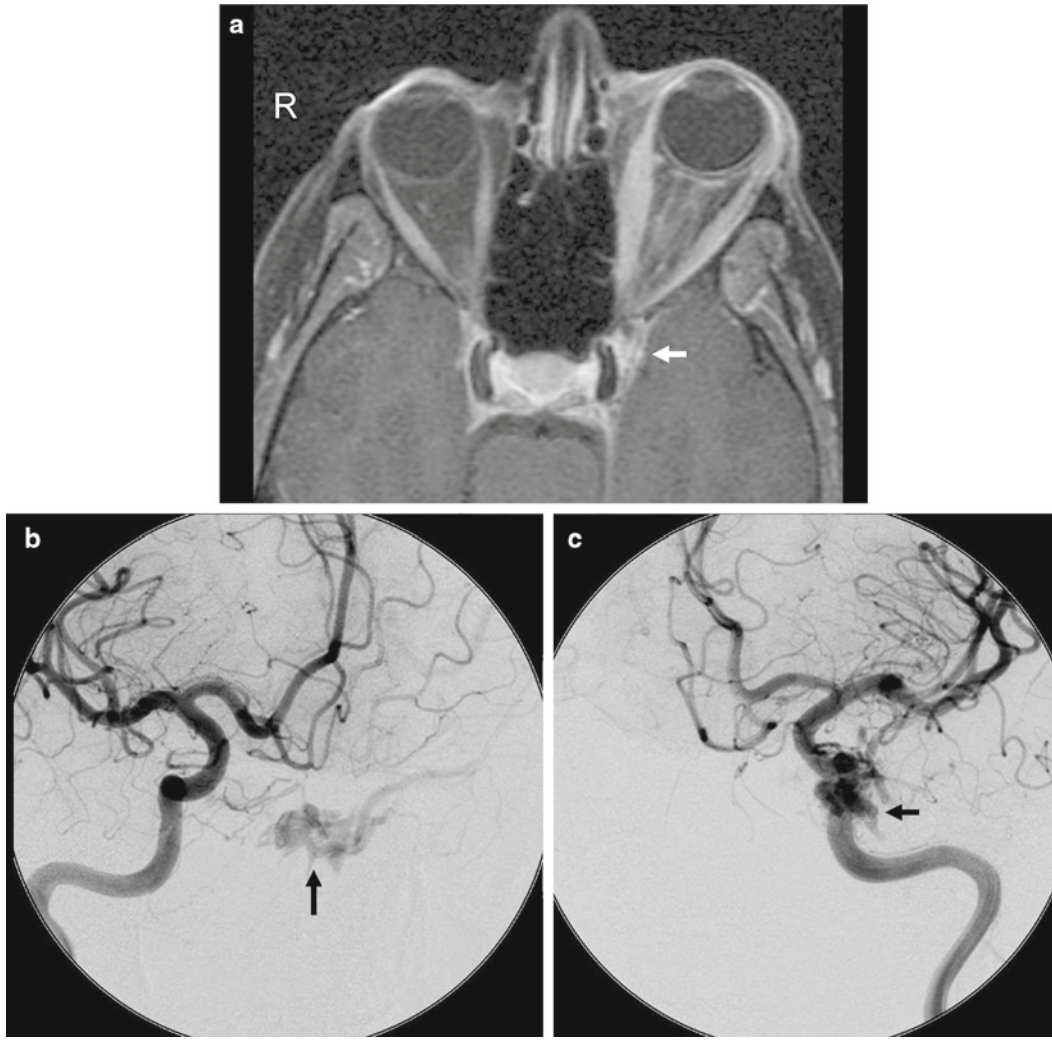


**Fig. 2.24** Left CCF. (**a**) Axial T1-weighted post-contrast with fat suppression image demonstrates left proptosis, enlargement of the left extraocular muscles, and slight asymmetric fullness of the left cavernous sinus. (**b** and **c**) Catheter cerebral angiogram from selective right (**b**) and left (**c**) ICA injections show abnormal filling of the left cavernous sinus, confirming a left CCF (*arrow*)

connect the cavernous sinuses. In severe cases, intracranial venous hypertension can lead to brain edema and hemorrhagic venous infarction. Skull base fractures, especially those involving the sphenoid bone, should alert the clinicians to search for associated cavernous carotid injury. Patients can present weeks or even months after the initial trauma. Therefore, a CCF can be overlooked if a detailed clinical history and ophthalmic examination are not performed.

The *dural arteriovenous fistula* (DAVF) is most often caused by laceration of the middle meningeal artery with resultant meningeal artery to meningeal vein fistulous communication (Fig. 2.25). Because the fistula generally drains via the meningeal veins, the injured middle miningeal artery rarely leads to the formation of an EDH. Patients are often asymptomatic or present with nonspecific complaints such as tinnitus.

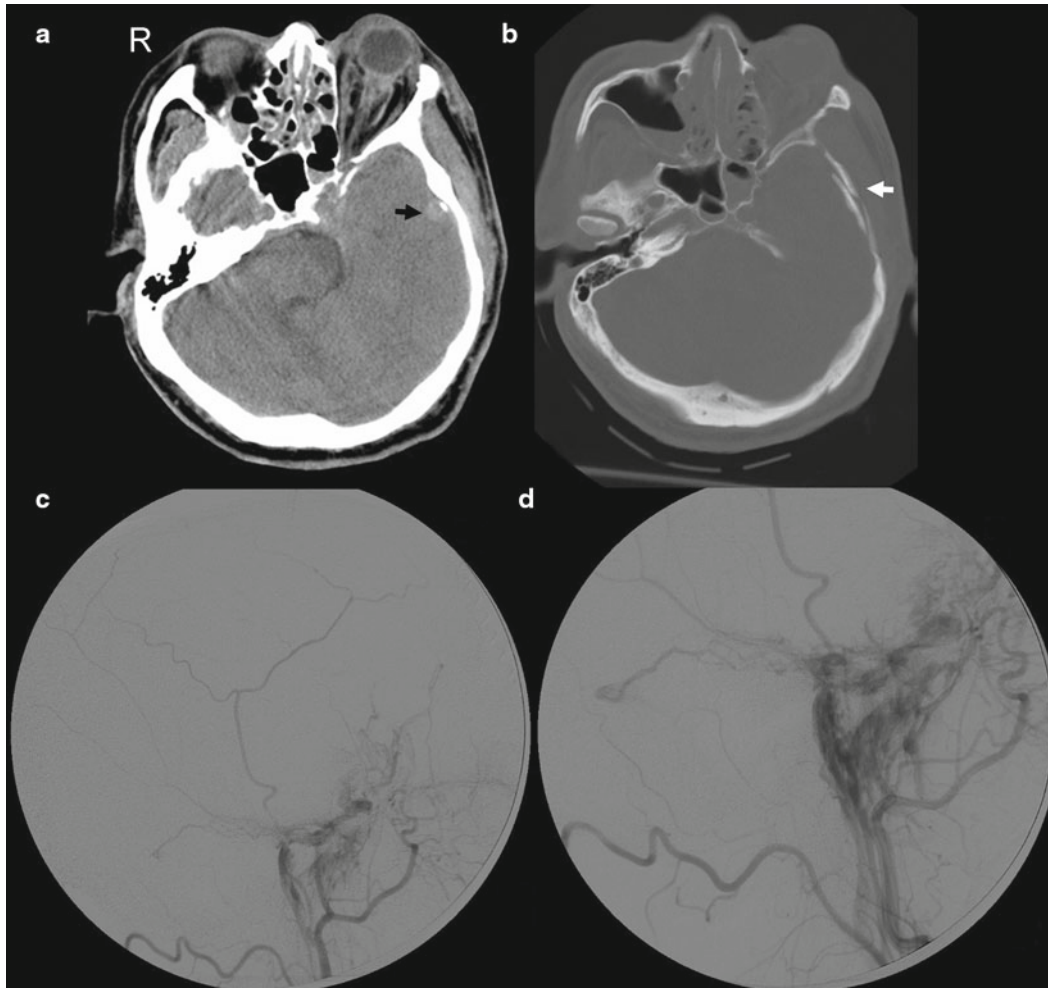


**Fig. 2.25** Dural arteriovenous fistula (DAVF). (**a**) Axial CT image displayed in "soft tissue window" shows a small, round, dense, left temporal extra-axial focus (*arrow*). There is also left orbital proptosis and retrobulbar soft tissue stranding. (**b**) Corresponding "bone window" image shows a fracture of the squamosal portion of the left temporal bone (*arrow*). (**c** and **d**) Images from an external carotid artery catheter angiogram in the lateral projection show an abnormal blush of contrast due to a dural AVF with filling of the middle meningeal vein via the middle meningeal artery. (Reprinted with permission from Le TH and Gean AD. Neuroimaging of traumatic brain injury. Mt Sinai J Med. 2009;76:145–162)

## Acute Secondary Injury

### Cerebral Swelling

*Cerebral swelling* refers to an increase in cerebral volume which can develop from an increase in tissue blood volume (*hyperemia*) or an increase in tissue fluid (*cerebral edema*). Cerebral edema can be further divided into five major subtypes: vasogenic, cytotoxic, hydrostatic, hypo-osmotic, and interstitial. Among these subtypes, vasogenic edema is the most common in TBI. Hyperemia and vasogenic edema are thought to be the result of cerebral dysautoregulation. Cytotoxic edema is believed to occur secondary to tissue hypoxia. Hydrostatic edema occurs from a sudden increase in intravascular pressure, and can be seen with sudden decompression of a focal mass. Hypo-osmotic edema is caused by a decrease in serum osmolality, with subsequent efflux of fluid from the intravascular to the extravascular space. Interstitial edema occurs from movement of fluid into the periventricular space secondary to obstructive hydrocephalus.

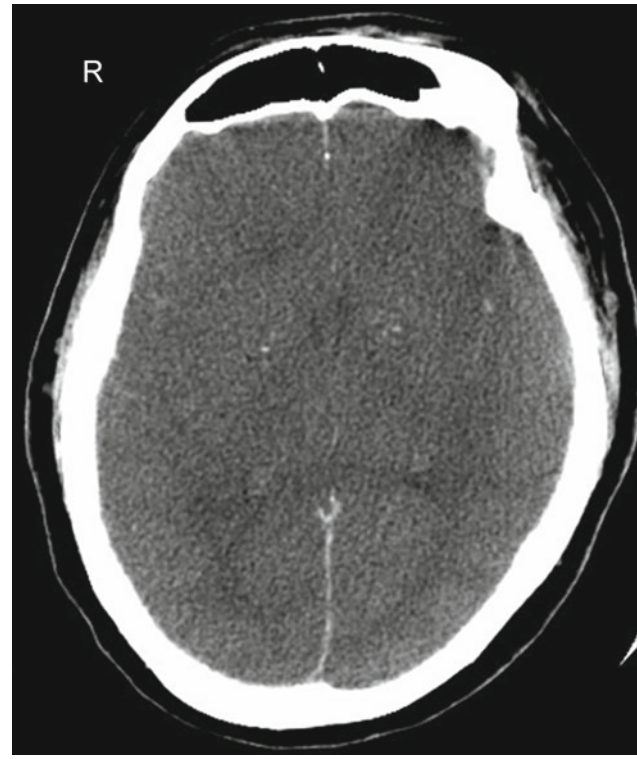


**Fig. 2.26** Cerebral edema and DAI. Non-contrast axial CT image demonstrates diffuse effacement of the cerebral sulci and diffuse loss of gray-white matter differentiation due to diffuse cerebral edema. Multiple foci of shear hemorrhages within the left temporal lobe are also visible, indicating acute hemorrhagic DAI

Effacement of the cerebral sulci and cisterns, as well as compression of the ventricles, are typical imaging findings (Fig. 2.26). In cytotoxic edema, the gray-white differentiation is lost, which is in contrast to hyperemia and vasogenic edema where the gray-white differentiation is preserved. Even with cytotoxic edema, the cerebellum and brainstem are usually spared and may appear hyperintense relative to the affected cerebral hemispheres.

### Brain Herniation

Traumatic *brain herniation* refers to displacement of brain tissue from one compartment to another secondary to mass effect produced either by primary or secondary injuries. The compartmentalization is based on the dural partitions and skull openings. In *subfalcine* herniation, the cingulate gyrus is displaced across the midline under the falx cerebri and above the corpus callosum (Figs. 2.8b and 2.10a). Compression of the ipsilateral ventricle due to mass effect and enlargement of the contralateral ventricle due to obstruction of the foramen of Monro can be seen on imaging. In *uncal* herniation, the medial temporal lobe is displaced over the free margin of the tentorium. Effacement of the lateral aspect of the suprasellar cisterns is an important early clue indicating the presence of uncal herniation. In *transtentorial* herniation, the brain herniates either upward or downward. Upward herniation occurs when portions of the cerebellum and vermis displace through the tentorial incisura. In posterior fossa downward herniation, the cerebellar tonsils displace through the foramen magnum. Downward herniation of the cerebrum manifests as effacement of the suprasellar and perimesencephalic cisterns. Inferior displacement of the calcified pineal gland is another clue for the presence of downward herniation. *External* herniation occurs when elevated ICP is combined with a skull defect (Figs. 2.8b and 2.28b). External herniation is observed more frequently due to an increased use of decompressive craniectomies. With all types of brain herniation, the underlying culprit must be corrected in a timely fashion to prevent further secondary injury.

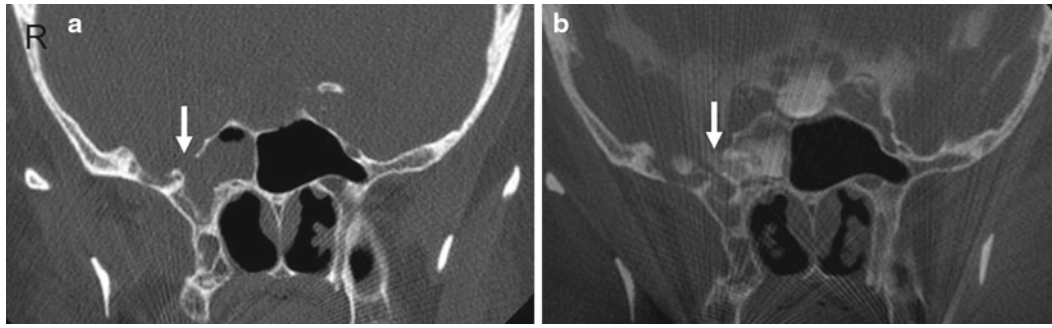


**Fig. 2.27** CSF leak. (**a**) Coronal CT image shows a bony defect of the right sphenoid sinus (*arrow*). (**b**) Coronal CT image from a cisternogram shows leakage of contrast into the right sphenoid sinus through the bony defect. (Reprinted with permission from Le TH and Gean AD. Neuroimaging of traumatic brain injury. Mt Sinai J Med. 2009;76:145–162)

### Ischemia and Infarction

*Ischemia and infarction* can result from vascular injury, diffuse increase in ICP, cytotoxic cerebral edema, or focal compressive mass effect on cerebral vasculature by herniation or hematoma. With subfalcine herniation, the anterior cerebral arteries (ACA) are displaced to the contralateral side, trapping the callosomarginal branches of the ACA, leading to ACA infarction. In severe uncal herniation, displacement of the brainstem can compress the contralateral cerebral peduncle and the posterior cerebral artery (PCA) against the tentorium ("*Kernohan's notch*"), leading to peduncular infarction and/or PCA infarction. Tonsillar herniation can cause ischemia in the territory of the posterior inferior cerebellar artery.

## Chronic Secondary Injury

### Hydrocephalus

Traumatic *hydrocephalus* develops due to impaired CSF reabsorption at the level of the arachnoid villi (*communicating hydrocephalus*) or due to intraventricular obstruction (*non-communicating hydrocephalus*), usually at the level of the cerebral aqueduct. Mass effect from brain herniation or a hematoma can also cause non-communicating hydrocephalus via compression of the aqueduct, foramen of Monro, or ventricular outflow foramina. Hydrocephalus commonly develops as a complication of prior SAH or IVH. On imaging, the ventricles are dilated, the sulci may be effaced, and periventricular transependymal interstitial edema may occur.

### Cerebralspinal Fluid Leak

The *cerebrospinal fluid (CSF) leak* occurs from a dural tear and an associated skull base fracture. The dural tear results in communication between the intra- and extra-dural spaces. Communication between the subarachnoid space and middle ear, in association with a ruptured tympanic membrane, causes CSF otorrhea. Similarly, communication between the subarachnoid space and the paranasal sinuses causes CSF rhinorrhea. In patients with recurrent meningeal infections, a CSF leak should be suspected. CSF leaks are often difficult to localize. Radionuclide cisternography is highly sensitive for the detection of CSF leak (Curnes et al. 1985). However, CT scanning with intrathecal contrast is often required for detailed anatomic localization of the defect (Fig. 2.27) (La Fata et al. 2008).

## Blast-Induced Injury

Blast-induced TBI is brain injury generated by an explosion. Blast-induced TBI deserves special emphasis since it is considered the "*signature wound of the current war on terror*" (Neuroscience 2008) due to an increasing use of improvised explosive devices (IEDs) in terrorist and insurgent activities. Blast injuries can be classified as *primary, secondary, tertiary, or quaternary*. *Primary blast injuries* are due to an over-pressurization shock wave. The brain, surrounded by cerebral fluid, is especially susceptible to primary blast

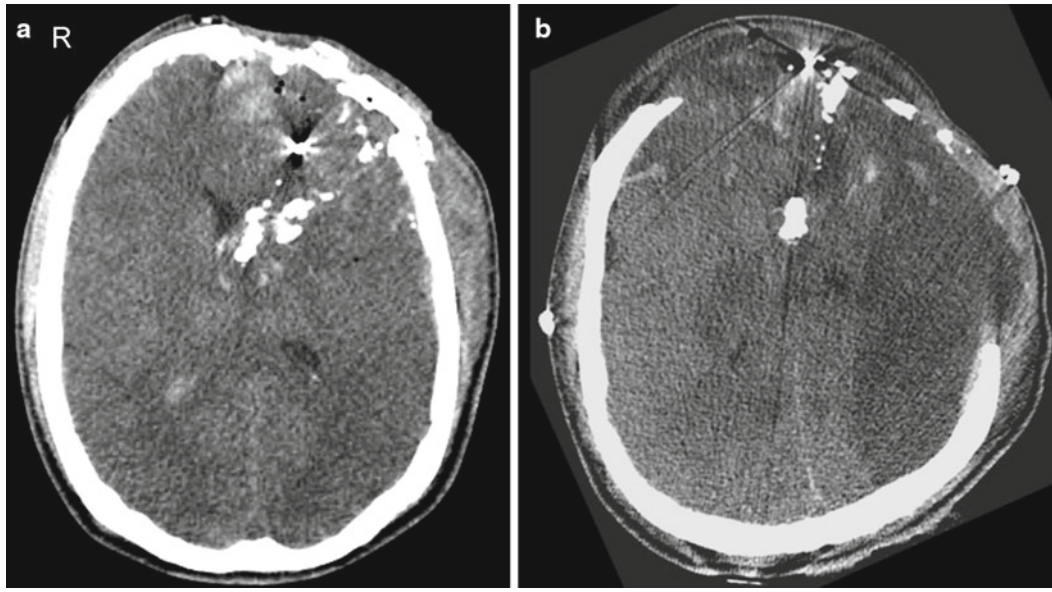


**Fig. 2.28** Blast-induced TBI. (**a**) Non-contrast axial CT images show multiple metallic fragments, comminuted left frontal fractures, left frontal pneumocephalus, and left frontal scalp soft-tissue swelling. High-density collection within the occipital horn of the right lateral ventricle indicates acute IVH. (**b**) Follow-up CT, performed after decompressive craniectomy, reveals left frontal external herniation. There is diffuse decrease in attenuation of the left frontal lobe and loss of gray-white differentiation from secondary ischemic injury. There is also diffuse effacement of the cerebral sulci from cerebral edema. Bilateral anterior frontal low attenuation also indicates ischemic changes in these regions

injury (Elsayed 1997; Elsayed et al. 1997; Mayorga 1997). *Secondary blast injuries* are caused by bomb fragments and other objects propelled by the explosion, resulting in penetrating injuries. *Tertiary blast injuries* result when a person becomes a missile and is thrown against other objects. Therefore, tertiary blast injuries are similar to those that occur in blunt trauma. *Quaternary blast injuries* are all other injuries not included in the first three classes. The manifestation of blast injury on the brain is usually a combination of the different classes of blast injury (Fig. 2.28). Brain injuries acquired from the explosion often develop cerebral edema, subarachnoid hemorrhage, and vasospasm (Fig. 2.29).

## Summary

Diagnosis and management of TBI requires a multi-disciplinary approach. The goals of imaging in TBI involve identifying treatable injuries, assisting in the prevention of secondary damage, and providing useful prognostic information. While progress in medical imaging technology has resulted in an increase in multiple imaging methods, leading to improvement in early detection of TBI and adding useful prognostic information, CT still remains the imaging modality of choice in the acute setting because it is fast, widely accessible, and has few contraindications. MRI is indicated in the acute setting if the neurologic findings are unexplained by the CT findings. MRI is preferred over CT for subacute and chronic TBI because of its superior sensitivity to older blood products and to both gray and white matter injury. Novel MRI methods, such as DWI, SWI, MRS, MTI and perfusion MRI, further improve the sensitivity of MRI in detecting TBI lesions, and can add valuable prognostic information. PET and MSI show promise in the evaluation of TBI, although their availability is limited due to cost. Continuing research and development in imaging will enhance our understanding of the pathophysiological manifestations of brain trauma and further improve clinical management of TBI.

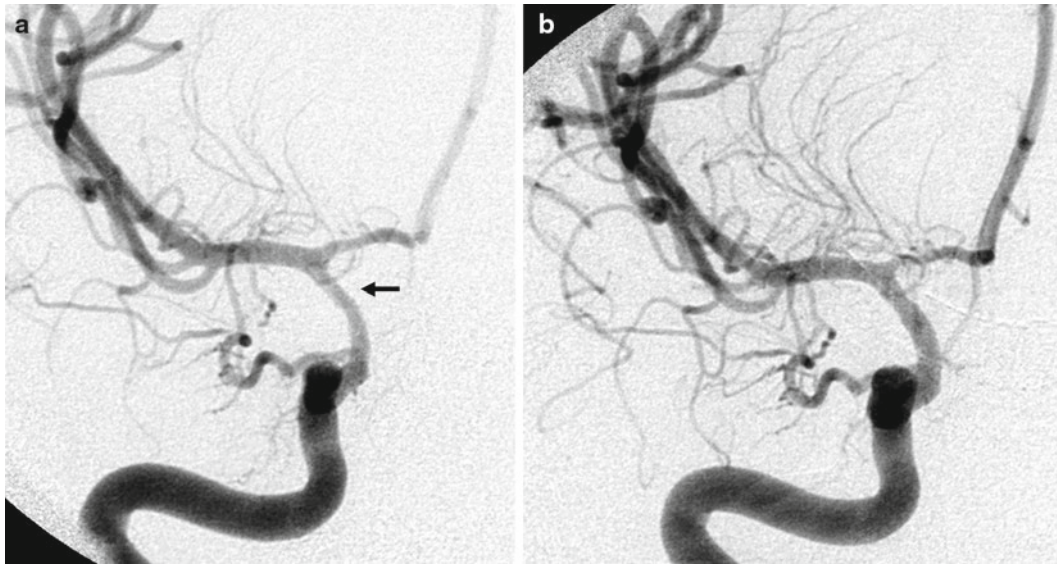


**Fig. 2.29** Blast-induced vasopasm pre- and post-angioplasty. (**a**) Catheter cerebral angiogram from a selective left ICA injection, of the same patient in Fig. 2.28, shows mild narrowing and irregularity of the supraclinoid left ICA (*arrow*) due to vasospasm. (**b**) Follow-up angiogram post-angioplasty shows improvement in the irregularity and narrowing. (Courtesy of Rocco Armonda, M.D., Washington Hospital Center, Washington, DC)

**Acknowledgments** We thank the residents, fellows, and attendings from the Neuroradiology Section of the University of California, San Francisco for their continuing effort to submit interesting cases to the teaching file server (http://tfserver.ucsf.edu). Some of the cases presented in this article were the product of their contributions.

## References

Adams J. Pathology of nonmissile head injury. Neuroimaging Clin N Am. 1991;1:397–410.

Adams JH, Graham DI, Gennarelli TA, Maxwell WL. Diffuse axonal injury in non-missile head injury. J Neurol Neurosurg Psychiatry. 1991;54(6):481–3.

Al-Nakshabandi NA. The swirl sign. Radiology. 2001; 218(2):433.

Arfanakis K, Haughton VM, Carew JD, Rogers BP, Dempsey RJ, Meyerand ME. Diffusion tensor MR imaging in diffuse axonal injury. AJNR Am J Neuroradiol. 2002;23(5):794–802.

Ashikaga R, Araki Y, Ishida O. MRI of head injury using FLAIR. Neuroradiology. 1997;39(4):239–42.

Awasthi D. Civilian gunshot wounds to the head. Proceedings of the American Association of Neurological Surgeons. San Francisco; 1992.

Babikian T, Freier MC, Tong KA, et al. Susceptibility weighted imaging: neuropsychologic outcome and pediatric head injury. Pediatr Neurol. 2005;33(3): 184–94.

Bell RS, Loop JW. The utility and futility of radiographic skull examination for trauma. N Engl J Med. 1971;284(5):236–9.

Bergsneider M, Hovda DA, McArthur DL, et al. Metabolic recovery following human traumatic brain injury based on FDG-PET: time course and relationship to neurological disability. J Head Trauma Rehabil. 2001;16(2):135–48.

Briggs M. Traumatic pneumocephalus. Br J Surg. 1974;61(4):307–12.

Coles JP, Fryer TD, Smielewski P, et al. Incidence and mechanisms of cerebral ischemia in early clinical head injury. J Cereb Blood Flow Metab. 2004a;24(2): 202–11.

Coles JP, Fryer TD, Smielewski P, et al. Defining ischemic burden after traumatic brain injury using 15O PET imaging of cerebral physiology. J Cereb Blood Flow Metab. 2004b;24(2):191–201.

Conturo TE, Lori NF, Cull TS, et al. Tracking neuronal fiber pathways in the living human brain. Proc Natl Acad Sci USA. 1999;96(18):10422–7.

Curnes JT, Vincent LM, Kowalsky RJ, McCartney WH, Staab EV. CSF rhinorrhea: detection and localization using overpressure cisternography with Tc-99 m-DTPA. Radiology. 1985;154(3):795–9.

Dubey A, Sung WS, Chen YY, et al. Traumatic intracranial aneurysm: a brief review. J Clin Neurosci. 2008; 15(6):609–12.

Elsayed NM. Toxicology of blast overpressure. Toxicology. 1997;121(1):1–15.

Elsayed NM, Gorbunov NV, Kagan VE. A proposed biochemical mechanism involving hemoglobin for blast

overpressure-induced injury. Toxicology. 1997;121(1): 81–90.
Enterline DS, Kapoor G. A practical approach to CT angiography of the neck and brain. Tech Vasc Interv Radiol. 2006;9(4):192–204.
Fobben ES, Grossman RI, Atlas SW, et al. MR characteristics of subdural hematomas and hygromas at 1.5T. AJR Am J Roentgenol. 1989;153(3):589–95.
Frigon C, Jardine DS, Weinberger E, Heckbert SR, Shaw DW. Fraction of inspired oxygen in relation to cerebrospinal fluid hyperintensity on FLAIR MR imaging of the brain in children and young adults undergoing anesthesia. AJR Am J Roentgenol. 2002;179(3): 791–6.
Garnett MR, Blamire AM, Corkill RG, Cadoux-Hudson TA, Rajagopalan B, Styles P. Early proton magnetic resonance spectroscopy in normal-appearing brain correlates with outcome in patients following traumatic brain injury. Brain. 2000a;123(Pt 10):2046–54.
Garnett MR, Blamire AM, Rajagopalan B, Styles P, Cadoux-Hudson TA. Evidence for cellular damage in normal-appearing white matter correlates with injury severity in patients following traumatic brain injury: a magnetic resonance spectroscopy study. Brain. 2000b;123(Pt 7):1403–9.
Gean AD, Kates RS, Lee S. Neuroimaging in head injury. New Horiz. 1995;3(3):549–61.
Gennarelli TA, Thibault LE, Adams JH, Graham DI, Thompson CJ, Marcincin RP. Diffuse axonal injury and traumatic coma in the primate. Ann Neurol. 1982;12(6):564–74.
Gentry LR. Head trauma. In: Atlas SW, editor. Magnetic resonance imaging of the brain and spine. 2nd ed. Philadelphia, PA: Lippincott-Raven; 1996. p. 611–47.
Gentry LR, Godersky JC, Thompson B, Dunn VD. Prospective comparative study of intermediate-field MR and CT in the evaluation of closed head trauma. AJR Am J Roentgenol. 1988;150(3):673–82.
Gomori JM, Grossman RI, Goldberg HI, Zimmerman RA, Bilaniuk LT. Intracranial hematomas: imaging by high-field MR. Radiology. 1985;157(1):87–93.
Greenberg J, Cohen WA, Cooper PR. The "hyperacute" extraaxial intracranial hematoma: computed tomographic findings and clinical significance. Neurosurgery. 1985;17(1):48–56.
Haacke EM, Xu Y, Cheng YC, Reichenbach JR. Susceptibility weighted imaging (SWI). Magn Reson Med. 2004;52(3):612–8.
Hackney DB. Skull radiography in the evaluation of acute head trauma: a survey of current practice. Radiology. 1991;181(3):711–4.
Hardwood-Nash DC, Fritz CR. Neuroradiology in infants and children. St. Louis, MO: CV Mosby; 1976.
Haydel MJ, Preston CA, Mills TJ, Luber S, Blaudeau E, DeBlieux PM. Indications for computed tomography in patients with minor head injury. N Engl J Med. 2000;343(2):100–5.
Hesselink JR, Dowd CF, Healy ME, Hajek P, Baker LL, Luerssen TG. MR imaging of brain contusions: a comparative study with CT. AJR Am J Roentgenol. 1988;150(5):1133–42.
Huisman TA, Sorensen AG, Hergan K, Gonzalez RG, Schaefer PW. Diffusion-weighted imaging for the evaluation of diffuse axonal injury in closed head injury. J Comput Assist Tomogr. 2003;27(1):5–11.
Inglese M, Makani S, Johnson G, et al. Diffuse axonal injury in mild traumatic brain injury: a diffusion tensor imaging study. J Neurosurg. 2005;103(2):298–303.
Jagoda AS, Cantrill SV, Wears RL, et al. Clinical policy: neuroimaging and decisionmaking in adult mild traumatic brain injury in the acute setting. Ann Emerg Med. 2002;40(2):231–49.
Jennett B, Adams JH, Murray LS, Graham DI. Neuropathology in vegetative and severely disabled patients after head injury. Neurology. 2001;56(4): 486–90.
Kato T, Nakayama N, Yasokawa Y, Okumura A, Shinoda J, Iwama T. Statistical image analysis of cerebral glucose metabolism in patients with cognitive impairment following diffuse traumatic brain injury. J Neurotrauma. 2007;24(6):919–26.
Kinuya K, Kakuda K, Nobata K, et al. Role of brain perfusion single-photon emission tomography in traumatic head injury. Nucl Med Commun. 2004;25(4): 333–7.
Kumbhani SR, Purcell DD, Gean AD. Contrast extravasation within a traumatic epidural hematoma: have we been missing something? Paper presented at: American Society of Neuroradiology 47th annual meeting & NER Foundation symposium 2009. Vancouver, Canada; 16–21 May, 2009.
La Fata V, McLean N, Wise SK, DelGaudio JM, Hudgins PA. CSF leaks: correlation of high-resolution CT and multiplanar reformations with intraoperative endoscopic findings. AJNR Am J Neuroradiol. 2008;29(3): 536–41.
Le TH, Gean AD. Neuroimaging of traumatic brain injury. Mt Sinai J Med. 2009;76(2):145–62.
Le TH, Mukherjee P, Henry RG, Berman JI, Ware M, Manley GT. Diffusion tensor imaging with three-dimensional fiber tractography of traumatic axonal shearing injury: an imaging correlate for the posterior callosal "disconnection" syndrome: case report. Neurosurgery. 2005;56(1):189.
Lee H, Wintermark M, Gean AD, Ghajar J, Manley GT, Mukherjee P. Focal lesions in acute mild traumatic brain injury and neurocognitive outcome: CT versus 3T MRI. J Neurotrauma. 2008;25(9):1049–56.
Lewine JD, Davis JT, Sloan JH, Kodituwakku PW, Orrison Jr WW. Neuromagnetic assessment of pathophysiologic brain activity induced by minor head trauma. AJNR Am J Neuroradiol. 1999;20(5): 857–66.
Lewine JD, Davis JT, Bigler ED, et al. Objective documentation of traumatic brain injury subsequent to mild head trauma: multimodal brain imaging with MEG, SPECT, and MRI. J Head Trauma Rehabil. 2007; 22(3):141–55.

Lindenberg R, Freytag E. The mechanism of cerebral contusions. A pathologic-anatomic study. Arch Pathol. 1960;69:440–69.

Lipper MH, Kishore PR, Girevendulis AK, Miller JD, Becker DP. Delayed intracranial hematoma in patients with severe head injury. Radiology. 1979;133(3 Pt 1): 645–9.

Liu AY, Maldjian JA, Bagley LJ, Sinson GP, Grossman RI. Traumatic brain injury: diffusion-weighted MR imaging findings. AJNR Am J Neuroradiol. 1999; 20(9):1636–41.

Masters SJ. Evaluation of head trauma: efficacy of skull films. AJR Am J Roentgenol. 1980;135(3):539–47.

Mayorga MA. The pathology of primary blast overpressure injury. Toxicology. 1997;121(1):17–28.

Menon DK. Brain ischaemia after traumatic brain injury: lessons from 15O2 positron emission tomography. Curr Opin Crit Care. 2006;12(2):85–9.

Messori A, Polonara G, Mabiglia C, Salvolini U. Is haemosiderin visible indefinitely on gradient-echo MRI following traumatic intracerebral haemorrhage? Neuroradiology. 2003;45(12):881–6.

Mittl RL, Grossman RI, Hiehle JF, et al. Prevalence of MR evidence of diffuse axonal injury in patients with mild head injury and normal head CT findings. AJNR Am J Neuroradiol. 1994;15(8):1583–9.

Mori S, van Zijl P. Fiber tracking: principles and strategies—a technical review. NMR Biomed. 2002;15: 468–80.

Munoz-Sanchez MA, Murillo-Cabezas F, Cayuela-Dominguez A, Rincon-Ferrari MD, Amaya-Villar R, Leon-Carrion J. Skull fracture, with or without clinical signs, in mTBI is an independent risk marker for neurosurgically relevant intracranial lesion: a cohort study. Brain Inj. 2009;23(1):39–44.

Nakashima T, Nakayama N, Miwa K, Okumura A, Soeda A, Iwama T. Focal brain glucose hypometabolism in patients with neuropsychologic deficits after diffuse axonal injury. AJNR Am J Neuroradiol. 2007;28(2):236–42.

Nanassis K, Frowein RA, Karimi A, Thun F. Delayed post-traumatic intracerebral bleeding. Delayed post-traumatic apoplexy: "Spatapoplexie". Neurosurg Rev. 1989;12 Suppl 1:243–51.

Bhattacharjee Y. Neuroscience. Shell shock revisited: solving the puzzle of blast trauma. Science. 2008;319(5862):406–8.

Newton MR, Greenwood RJ, Britton KE, et al. A study comparing SPECT with CT and MRI after closed head injury. J Neurol Neurosurg Psychiatry. 1992;55(2): 92–4.

Niogi SN, Mukherjee P, Ghajar J, et al. Extent of microstructural white matter injury in postconcussive syndrome correlates with impaired cognitive reaction time: a 3T diffusion tensor imaging study of mild traumatic brain injury. AJNR Am J Neuroradiol. 2008;29(5):967–73.

Noguchi K, Ogawa T, Seto H, et al. Subacute and chronic subarachnoid hemorrhage: diagnosis with fluid-attenuated inversion-recovery MR imaging. Radiology. 1997;203(1): 257–62.

Orrison WW, Gentry LR, Stimac GK, Tarrel RM, Espinosa MC, Cobb LC. Blinded comparison of cranial CT and MR in closed head injury evaluation. AJNR Am J Neuroradiol. 1994;15(2):351–6.

Pruthi N, Balasubramaniam A, Chandramouli BA, et al. Mixed-density extradural hematomas on computed tomography-prognostic significance. Surg Neurol. 2009;71(2):202–6.

Purvis JT. Craniocerebral injuries due to missiles and fragments. Head injury conference proceedings. Philadelphia; 1966.

Reilly PL, Graham DI, Adams JH, Jennett B. Patients with head injury who talk and die. Lancet. 1975; 2(7931):375–7.

Siebert E, Bohner G, Dewey M, et al. 320-slice CT neuroimaging: initial clinical experience and image quality evaluation. Br J Radiol. 2009;82(979): 561–70.

Sinson G, Bagley LJ, Cecil KM, et al. Magnetization transfer imaging and proton MR spectroscopy in the evaluation of axonal injury: correlation with clinical outcome after traumatic brain injury. AJNR Am J Neuroradiol. 2001;22(1):143–51.

Soloniuk D, Pitts LH, Lovely M, Bartkowski H. Traumatic intracerebral hematomas: timing of appearance and indications for operative removal. J Trauma. 1986; 26(9):787–94.

Stiell IG, Lesiuk H, Wells GA, et al. Canadian CT head rule study for patients with minor head injury: methodology for phase II (validation and economic analysis). Ann Emerg Med. 2001a;38(3):317–22.

Stiell IG, Lesiuk H, Wells GA, et al. The Canadian CT Head Rule Study for patients with minor head injury: rationale, objectives, and methodology for phase I (derivation). Ann Emerg Med. 2001b;38(2):160–9.

Stiell IG, Wells GA, Vandemheen K, et al. The Canadian CT Head Rule for patients with minor head injury. Lancet. 2001c;357(9266):1391–6.

Teasdale G, Jennett B. Assessment of coma and impaired consciousness. A practical scale. Lancet. 1974;2(7872): 81–4.

Tong KA, Ashwal S, Holshouser BA, et al. Hemorrhagic shearing lesions in children and adolescents with posttraumatic diffuse axonal injury: improved detection and initial results. Radiology. 2003;227(2): 332–9.

Tong KA, Ashwal S, Holshouser BA, et al. Diffuse axonal injury in children: clinical correlation with hemorrhagic lesions. Ann Neurol. 2004;56(1):36–50.

Vertinsky AT, Schwartz NE, Fischbein NJ, Rosenberg J, Albers GW, Zaharchuk G. Comparison of multidetector CT angiography and MR imaging of cervical artery dissection. AJNR Am J Neuroradiol. 2008;29(9): 1753–60.

Wintermark M, van Melle G, Schnyder P, et al. Admission perfusion CT: prognostic value in patients with severe head trauma. Radiology. 2004;232(1):211–20.

Wintermark M, Sesay M, Barbier E, et al. Comparative overview of brain perfusion imaging techniques. Stroke. 2005;36(9):e83–99.

Woodcock Jr RJ, Short J, Do HM, Jensen ME, Kallmes DF. Imaging of acute subarachnoid hemorrhage with a fluid-attenuated inversion recovery sequence in an animal model: comparison with non-contrast-enhanced CT. AJNR Am J Neuroradiol. 2001;22(9): 1698–703.

Youn SW, Kim JH, Weon YC, Kim SH, Han MK, Bae HJ. Perfusion CT of the brain using 40-mm-wide detector and toggling table technique for initial imaging of acute stroke. AJR Am J Roentgenol. 2008;191(3): W120–6.

Zee CS, Go JL. CT of head trauma. Neuroimaging Clin N Am. 1998;8(3):525–39.

Zimmerman RA, Bilaniuk LT, Bruce D, Dolinskas C, Obrist W, Kuhl D. Computed tomography of pediatric head trauma: acute general cerebral swelling. Radiology. 1978;126(2):403–8.